# The Gulf of Mexico and ENSO Influence on Subseasonal and Seasonal CONUS Winter Tornado Variability

MARIA J. MOLINA AND JOHN T. ALLEN

*Department of Earth and Atmospheric Sciences, Central Michigan University, Mount Pleasant, Michigan*

VITTORIO A. GENSINI

*Department of Geographic and Atmospheric Sciences, Northern Illinois University, DeKalb, Illinois*

## ABSTRACT

El Niño–Southern Oscillation (ENSO) and the Gulf of Mexico (GoM) influence winter tornado variability and significant tornado (EF2+, where EF is the enhanced Fujita scale) environments. Increases occur in the probability of a significant tornado environment from the southern Great Plains to the Midwest during La Niña, and across the southern contiguous United States (CONUS) during El Niño. Winter significant tornado environments are absent across Florida, Georgia, and the coastal Carolinas during moderate-to-strong La Niña events. Jet stream modulation by ENSO contributes to higher tornado totals during El Niño in December and La Niña in January, especially when simultaneous with a warm GoM. ENSO-neutral phases yield fewer and weaker tornadoes, but proximity to warm GoM climate features can enhance the probability of a significant tornado environment. ENSO intensity matters; stronger ENSO phases generate increases in tornado frequency and the probability of a significant tornado environment, but are characterized by large variance, in which very strong El Niño and La Niña events can produce unfavorable tornado climatological states. This study suggests that it is a feasible undertaking to expand spring seasonal and subseasonal tornado prediction efforts to encompass the winter season, which is of importance given the notable threat posed by winter tornadoes. Significant tornadoes account for 95% of tornado fatalities and winter tornadoes are rated significant more frequently than during other seasons.

## 1. Introduction

Studies considering the El Niño–Southern Oscillation (ENSO) relationship with winter [December–February (DJF)] tornadoes (Knowles and Pielke 2005; Allen et al. 2015; Cook et al. 2017) have neglected to examine the contribution from the Gulf of Mexico (GoM), an important low-level moisture source for DJF convective storms (Weiss 1992). The cool phase of ENSO (La Niña) has been associated with an increase in DJF tornadoes, while the warm phase (El Niño) has been related to decreases in DJF tornado frequency inland of Gulf Coast areas (Cook and Schaefer 2008; Allen et al. 2015). However, below- (above-) average tornadic activity has occurred during some strong DJF La Niña (El Niño) events, including those of 1988–89 and 1999–00 (1982–83 and 2015–16). GoM sea surface temperatures (SSTs) potentially

modulate DJF tornado seasonal frequency from the expected influence of ENSO. Subseasonally, the Storm Prediction Center (SPC) tornado database (Schaefer and Edwards 1999) contains considerable intraseasonal variability, not all of which is explained by ENSO. Furthermore, the densely populated southeastern region of the United States (SE-US; 25°–37°N, 93°–70°W) is disproportionately impacted by DJF tornadoes. The dense populations of the SE-US and poorly understood DJF tornadic variability raise concerns and serve as motivation to assess ENSO and the GoM as subseasonal and seasonal climate drivers of DJF tornadoes.

Modulations in tornadic activity based on ENSO phase are driven by physical mechanisms related to the jet stream. La Niña perturbs northward shifts in the position of the jet stream over the northern Pacific Ocean, increasing meridional flow downstream and enhancing cyclogenesis across the contiguous United States (CONUS) (Lee and Galway 1956; Ropelewski and Halpert 1986). Meanwhile, El Niño can intensify the subtropical jet

*Corresponding author*: Maria J. Molina, maria.janet.molina@gmail.com

stream over the Gulf Coast (Allen et al. 2015; Cook et al. 2017), resulting in a decreased spatial area receiving moist air advection from the GoM. These ENSO-induced variations in CONUS environments have been related to tornadic variability; La Niña (El Niño) leads to overall increases (decreases) in DJF tornado activity inland of the Gulf Coast (Tippett et al. 2015). However, substantial internal variability is present within each phase of ENSO and it is therefore possible that the degree of DJF tornado variability is related to ENSO intensity. ENSO-neutral phases have also been associated with more frequent days with large numbers of tornadoes when considering the months of January–March (Cook and Schaefer 2008; Cook et al. 2017). Conceivably, an "unmodulated" jet stream during ENSO-neutral conditions could favor severe convection if properly oriented shear profiles and buoyancy at low levels are present. Sufficient northward transport of low-level moisture from the GoM region can lead to tornado events ahead of transient baroclinic waves (Weiss 1992), but previous ENSO DJF tornadic variability studies have not explored the potential interrelationship with the GoM (e.g., Allen et al. 2015; Cook et al. 2017). Here, we hypothesize that the signal observed during ENSO-neutral years by Cook and Schaefer (2008) and Cook et al. (2017) could be in part from the GoM, and not solely due to neutral conditions of the tropical Pacific Ocean. Previous research relating cool-season tornado frequency and GoM SSTs supports this hypothesis; Edwards and Weiss (1996) found that increases (decreases) in DJF GoM SSTs were related to increases (decreases) in severe thunderstorm occurrences.

Challenges arise in exploring the relationship between the GoM and tornado variability. DJF GoM SSTs are not uniform across the basin, generally characterized by a north-to-south SST gradient of ~7°C due to increased cold-air intrusions, reduced solar radiation, and overall negative heat flux (Zavala-Hidalgo et al. 2002; Muller-Karger et al. 2015). The presence of GoM climate features, such as the Loop Current (LC), cold-core rings (CCRs), and/or warm-core rings (WCRs), can also lead to regions of anomalously warm or cold GoM SSTs (Vukovich 2007; Chang and Oey 2010). During return-flow events, GoM basin SST inhomogeneity could result in regional areas of enhanced or suppressed low-level buoyancy and severe thunderstorms, as Molina et al. (2016) found for the spring season. Moreover, GoM SSTs are not independent of the influence of ENSO. The aforementioned El Niño enhancement of the subtropical jet can lead to increased cloud cover and more frequent cold fronts traversing the GoM, both of which can contribute to cooler GoM SSTs (Ropelewski and Halpert 1986; Park and Leovy 2004). Conversely, La Niña can be conducive to GoM warming due to a northwardly

displaced polar jet (Montroy 1997; Barlow et al. 2001; Fye et al. 2004). The complex interplay between the GoM and ENSO, along with their individual contributions to convection, indicates that both should be considered as climate drivers of DJF tornadic activity despite challenges in isolating their respective signals.

From an exposure standpoint, cool-season tornadoes are infrequent and less thermodynamically favorable than warm-season events, typically associated with high shear and weak-to-moderate mixed-layer convective available potential energy (MLCAPE; $\leq 1000 \, \mathrm{J \, kg^{-1}}$) across southern states near the GoM (Galway and Pearson 1981; Smith et al. 2012; Sherburn and Parker 2014; King et al. 2017). Guyer et al. (2006) agreed that moderate-to-large amounts of MLCAPE are not necessary for DJF "significant" tornadoes (classified as EF2+ herein, on the enhanced Fujita scale[1]), but found their occurrence coincided with 0–3-km MLCAPE ($\geq 70 \, \mathrm{J \, kg^{-1}}$), suggesting some buoyancy at the lowest levels is still needed. Arguably, DJF significant tornado events are more sensitive to the limited atmospheric thermodynamics than kinematics. The southward seasonal migration of the polar jet and stronger subtropical jet makes a favorable kinematic vertical profile for cool-season tornadoes more common, generally of 0–6-km bulk wind shear (BWD) $\geq 45 \, \mathrm{kt}$ (where $1 \, \mathrm{kt} \approx 0.51 \, \mathrm{m \, s^{-1}}$) and 0–1-km BWD $\geq 20 \, \mathrm{kt}$ (Guyer et al. 2006). However, the presence of a favorable kinematic environment and some low-level instability is not a guarantee that a tornado will occur (Cohen et al. 2015, 2017). Efforts to identify parameters that aid in discriminating between nontornadic and tornadic events have yielded encouraging results (Brooks et al. 1994; Grams et al. 2012; Mercer et al. 2012) and include the significant tornado parameter (STP; Thompson et al. 2003).

Given the numerous constraints of the SPC tornado report dataset (Verbout et al. 2006; Doswell 2007; Doswell et al. 2009; Edwards et al. 2013), the use of STP as a significant tornado environment proxy is desirable. STP has been found to be a good discriminator between significant tornado producing supercells and nontornadic supercells, with values > 1 associated with most significant tornadoes (Thompson et al. 2003). Significant tornadoes are of particular importance in this study, given that they account for 95% of tornado fatalities despite encompassing 19% of all tornadoes (Schaefer and Edwards 1999). However, several limitations arise when using STP as a representation of DJF significant tornadoes. STP is calibrated to spring tornado environments of

---

[1] Tornado intensities were rated using the Fujita (F) scale (Fujita 1971) prior to 2007 (Potter 2007).

the Great Plains (Thompson et al. 2003) and may not identify tornado environments of other regions and/or seasons, such as the SE-US and/or DJF. In addition, the storm relative helicity variable in STP is designed to be used with discrete and right-moving supercells, but DJF convective modes also include quasi-linear convective systems (QLCS) and cell clusters (Thompson et al. 2003; Grams et al. 2012; Smith et al. 2012). Despite the aforementioned limitations, STP values of DJF Gulf Coast significant tornado events were found to be representative of significant tornado environments (Thompson et al. 2003; Guyer et al. 2006), demonstrating that its use for a DJF tornado climatology study is appropriate.

This paper is structured as follows. DJF tornado climatological characteristics are established by compositing report data using various categorical thresholds, with comparison to activity of other seasons in section 3a. DJF tornado and significant tornado environment variability in relation to the GoM and ENSO are explored in sections 3a(1) and 3a(2). Analysis of tornado frequency and environment modulation sensitivity to various ENSO intensities follows in 3a(3), with intensity thresholds delineated in section 2. Evaluation of the seasonal persistence of the relationship between the GoM, ENSO, and tornado activity was conducted using subseasonal analyses and is contained in section 3b, with focus on La Niña and El Niño in section 3b(1) and the GoM and ENSO in section 3b(2). Discussion of study result sensitivity to seasonal classification is included in section 3c, with concentration on result disparities between this study, Cook and Schaefer (2008), and Cook et al. (2017). Synoptic-scale atmospheric characteristics of two DJFs with unexplained tornado variability are considered in section 3d and potential relationships to alternative tropical Pacific indices in section 3e. Results are summarized in section 4, within the context of seasonal and subseasonal prediction efforts and the unique danger posed by DJF tornadic events.

## 2. Method

### a. Tornado report data

Tornado reports were obtained from the National Oceanic and Atmospheric Administration (NOAA) SPC severe report database (Schaefer and Edwards 1999; available online at http://www.spc.noaa.gov/wcm/). While the SPC database is the most reliable dataset of tornado reports available for the CONUS (Brooks and Doswell 2001), there are associated limitations that have been detailed in earlier studies (e.g., Verbout et al. 2006; Doswell et al. 2009; Edwards et al. 2013). Some issues are related to tornadoes of EF0 intensity, which exhibit a

nearly twofold increase during the 1990s due to an improvement in rating practices during that decade (Klazura and Imy 1993; Doswell 2007). In relation to long-term trends, Brooks et al. (2014) demonstrated that EF1+ tornadoes do not exhibit a significant trend and Schaefer et al. (2002) illustrated that the number of significant tornadoes has remained nearly constant. Therefore, in consideration of tornado report issues—and akin to earlier studies (e.g., Lee et al. 2016; Childs et al. 2018)—tornado report frequencies were restricted to EF1+ and significant tornadoes in this study.

Tornado days, defined as a day with a tornado of any intensity (EF0+), are less sensitive to changes of nonmeteorological origin across the temporal record (Brooks et al. 2003) and have been used in past tornado climatology studies to ameliorate SPC severe report database issues (e.g., Molina et al. 2016; Krocak and Brooks 2018). Therefore, in place of raw or detrended EF0+ tornado reports, tornado days were employed in this study, defined as a 24-h period beginning at 0000 UTC. Given the large number of fatalities associated with significant tornadoes, significant tornado days were also considered and defined as a day with an EF2+ tornado. Tornado days, significant tornado days, and EF1+ and significant tornado report frequencies were generated using the SPC database for DJF (December 1953–February 2016) for the SE-US and CONUS. The SPC severe report database dates back to 1950, but early years were omitted due to irregular reporting practices (Doswell and Burgess 1988; Verbout et al. 2006; Brooks et al. 2014). To establish a base climatology of DJF tornadoes within the annual cycle, DJF tornado frequencies were compared with tornado activity of other seasons. Seasons were stratified as spring [March–May (MAM)], summer [June–August (JJA)], and autumn [September–and November (SON)] from December 1953 through November 2016. Subseasonal tornado frequencies were also generated for the months of December, January, and February, to gain insight into the seasonal evolution of DJF.

### b. Environment data

Environmental proxies for severe thunderstorm occurrence are frequently used to substantiate results in studies that employ tornado report data (Tippett et al. 2015). As such, STP was used as a proxy for significant tornado occurrence in this study. North American Regional Reanalysis (NARR; Mesinger et al. 2006) data at 3-hourly temporal and 32-km horizontal grid spacing were used to derive STP for DJF (1981–2016). Gensini et al. (2014) found regional biases in NARR's representation of thermodynamic variables and surmised that surface-based parcel ascent choice can amend the

limitation. Thus, this study utilized STP composed of surface-based parcels, mirroring the formulation presented by Thompson et al. (2003) and used by Gensini and Marinaro (2016):

$$\text{STP} = \frac{\text{sbCAPE}}{1500\,\text{J kg}^{-1}} \times \frac{2000 - \text{sbLCL}}{1000\,\text{m}} \times \frac{0\text{--}1\text{kmSRH}}{150\,\text{m}^2\,\text{s}^{-2}}$$
$$\times \frac{0\text{--}6\,\text{kmBWD}}{20\,\text{m s}^{-1}}.$$

The surface-based lifting condensation level (sbLCL) term was set to zero if greater than 2000 m and 1.0 if less than 1000 m. The 0–6-km BWD was set to zero if less than $12.5\,\text{m s}^{-1}$ and 1.5 if greater than $30\,\text{m s}^{-1}$. In addition, STP was set to zero if the surface-based convective inhibition was less than $-125\,\text{J kg}^{-1}$. STP variable cutoff values are related to thresholds identified by previous studies (e.g., Brooks et al. 1994; Rasmussen and Blanchard 1998; Thompson et al. 2003), which aid in discriminating between tornadic and nontornadic supercells. Of interest in this study are the occurrences of STP > 1, associated with significant tornadoes (Thompson et al. 2003). Therefore, 3-h grid points with STP ≥ 1 were assigned values of 1, and 3-h grid points with STP < 1 were assigned values of zero. The binary classification of STP is referred to as mean STP 3-Hours, akin to the classification in Allen et al. (2018).

The oceanic Niño index (ONI; CPC 2015) was used to classify various ENSO phases and subsequently explore tornado and environment variability sensitivity to ENSO intensity during DJF. ONI uses a 3-month running average of extended reconstruction SSTs (ERSST.v5; Huang et al. 2017), with anomalies based on centered 30-yr base periods updated every 5 years to remove warming signals. ONI encapsulates SSTs of the Niño-3.4 region (5.0°S–5.0°N, 170.0°–120.0°W; Barnston et al. 1997) and is the index of choice in ENSO operational monitoring and prediction, given its ability to capture the oceanic component of ENSO (L'Heureux et al. 2015; Barnston et al. 2017). Thus, ONI was used to classify ENSO phases for most analyses in this study, with the exception of results in section 3e. ENSO phases were stratified as follows: ENSO neutral, $-0.5 < \text{ONI} < 0.5$; El Niño, ONI ≥ 0.5; La Niña, ONI ≤ $-0.5$; weak El Niño, $0.5 ≤ \text{ONI} < 1.0$; weak La Niña, $-1.0 < \text{ONI} ≤ -0.5$; moderate El Niño, $1.0 ≤ \text{ONI} < 1.5$; moderate La Niña, $-1.5 < \text{ONI} ≤ -1.0$; moderate-to-strong El Niño, ONI ≥ 1.0; moderate-to-strong La Niña, ONI ≤ $-1.0$; strong El Niño, ONI ≥ 1.5; and strong La Niña, ONI ≤ $-1.5$. DJF ONI was used for DJF seasonal analyses, NDJ ONI for December, DJF ONI for January, and JFM ONI for February. ONI data can be obtained online (http://www.cpc.ncep.noaa.gov/data/indices/oni.ascii.txt).

While ONI is an adequate index to use in classifying ENSO, there is no singular index that can capture the full range of ENSO internal variability and downstream impacts (L'Heureux et al. 2015). In addition, the 3-month running mean employed in ONI may smooth intraseasonal SST variability and reduce our ability to identify subseasonal signals in tornado frequency. Therefore, to explore potential teleconnections between the tropical Pacific and CONUS tornado activity, alternative indices were used, such as the Niño-3 region index (5.0°S–5.0°N, 150.0°–90.0°W), that are available online (CPC 2015). Monthly mean Niño-3 index values were used for subseasonal analyses and the 3-month mean of December–February was used for DJF. The Niño-3 region SSTAs are based on the 1981–2010 base period (CPC 2015). The Niño-4 region, Modoki (Ashok et al. 2007), and Niño-1+2 region indices were also explored in relation to DJF tornado variability, but produced weak and unclear relationships (not shown).

The covariance of SSTs and DJF tornado frequencies and environments was explored by generating composites using various percentiles of ranked tornado frequencies, ENSO phases, and SSTs as thresholds (e.g., 10th, 20th, 80th, and 90th percentiles). Subseasonal and seasonal area-averaged SST climatologies were determined using NOAA's National Centers for Environmental Information (NCEI) daily temporal and 0.25° spatial resolution data (available online at http://iridl.ldeo.columbia.edu/SOURCES/.NOAA/.NCDC/.OISST/.version2/.AVHRR/.sst/), which uses optimum interpolation (OISST) and Advanced Very High Resolution Radiometer (AVHRR) infrared satellite observations (Reynolds et al. 2007). SSTs were linearly detrended using least squares regression due to a warming signal observed in recent decades, particularly across the GoM (Allard et al. 2016). DJF SSTAs were calculated using a weekly base climatology from the available data time period (1981–2016), which limited the overall study temporal period.

While coarser SST datasets are available spanning a longer temporal record (e.g., ERSST.v5; Huang et al. 2017), the higher-resolution data (Reynolds et al. 2007) better resolve smaller-scale GoM features that are of importance to GoM climatology, such as the LC region (21.0°–28.0°N, 88.5°–82.5°W) and the WCR region (24.0°–29.0°N, 95.0°–87.0°W; Vukovich 2007). However, result confidence became a concern due to the limited sample size of certain composite runs (e.g., only ENSO-neutral years). Therefore, the monthly temporal and 2° spatial resolution NOAA ERSST.v5 dataset (Huang et al. 2017) was used from December 1953 through February 2016 for analysis of the entire GoM basin (18.5°–30.5°N, 98.0°–82.0°W), when deciphering smaller-scale GoM climate features is of lesser importance. The NOAA ERSST.v5

dataset (Huang et al. 2017) was detrended and anomalies calculated analogous to OISST AVHRR (Reynolds et al. 2007). Statistical significance ($\alpha = 0.05$) for all composite analyses was determined from a 20 000 member Monte Carlo distribution of bootstrap anomalies from the climatology.

Upon generating composite results for various ENSO phases, it became evident that the strong 1988–89 La Niña and 1997–98 El Niño departed from the expected relationship between ENSO and DJF tornado activity, resulting in below-average seasonal totals. DJF 300-hPa vector wind ($m\,s^{-1}$) and 500-hPa geopotential height (m) anomalies were computed for the 1988–89 La Niña and 1997–98 El Niño from the mean La Niña and mean El Niño climatologies (1979–2016), respectively. This was done to depict upper-level wind flow and midlevel geopotential height deviations from expected ENSO-related atmospheric circulation impacts across the Pacific Ocean (Bjerknes 1969). Anomalies detected could have contributed to downstream jet stream modulations that were unfavorable for tornadic activity. The National Centers for Environmental Predictions (NCEP)–Department of Energy (DOE) Atmospheric Model Intercomparison Project (AMIP-II) Reanalysis 2 (R-2) data at 6-hourly temporal and 2.5° horizontal resolution (Kanamitsu et al. 2002) were used to derive the atmospheric variables and are available online (http://www.esrl.noaa.gov/psd/). Statistical significance was evaluated similar to the aforementioned composites ($\alpha = 0.05$).

## 3. Results and discussion

### a. Winter seasonal tornado variability

Prior studies have described the elevated tornado risk inherent to DJF, particularly across the SE-US, which is due in part to increased nocturnal occurrence and SE-US population growth (e.g., Kis and Straka 2010; Ashley and Strader 2016). Here, we explore whether tornadoes that occur in DJF are rated significant more frequently than during other seasons, by computing the percentage of significant tornadoes from all intensity tornadoes stratified by season. It was found that more tornadoes are rated significant during DJF (26.8%), as compared with MAM (22.2%), JJA (13.6%), and SON (20.8%; not shown). The DJF season also contains the largest percentage of significant tornadoes per all intensity tornadoes when geographically constraining the area of interest to the SE-US (28.1%), as compared with MAM (26.5%), JJA (10.1%), and SON (20.0%; not shown). The southerly migrated polar jet, and thus more favorable vertical wind shear

climatological state, likely aid in the generation of the larger percentage of significant tornadoes in DJF as compared with other seasons. Overall, however, fewer EF1+ tornadoes have occurred in DJF as compared with other seasons; approximately 2900 EF1+ tornadoes have occurred in DJF as compared with 13 000 in MAM, 9900 in JJA, and 4500 in SON. The lower tornado frequency of DJF can also be appreciated in the numbers and percentages of tornado days and significant tornado days (Table 1, top half). The overall lack of low-level moisture and buoyancy make DJF tornadoes less climatologically likely, despite the more readily available favorable kinematics. Despite low tornado frequency, DJF is the second deadliest CONUS tornado season. This likely is due in part to the larger percentile of significant tornadoes (Table 1, top half). Additional factors also contribute to the aforementioned increased number of DJF tornado fatalities, such as the higher proportion of nocturnal tornadoes (Krocak and Brooks 2018) and increased mobile home exposure of the SE-US (Ashley 2007). The high mortality potential of DJF tornadoes underscores the importance of better understanding the relationship between the climate system and DJF severe thunderstorm variability.

Previous work has found that DJF tornado frequency increases inland of Gulf Coast areas during ENSO phases (e.g., Allen et al. 2015; Childs et al. 2018), which agrees with results identified herein. Most DJF tornadoes, tornado days, and significant tornado days occur during La Niña, followed by El Niño, as compared to ENSO-neutral phases across the CONUS and SE-US (Table 2). The relative lower frequency of DJF ENSO-neutral phase tornadoes coincides with weaker tornado intensities as well (Table 2). Importantly, however, La Niña and El Niño events have occurred more frequently than ENSO-neutral events during the study temporal period (DJF 1953–2016; Table 2).

In stratifying tornado occurrences by ONI, it becomes apparent that more CONUS and SE-US tornadoes and tornado days have occurred during weak and strong El Niño and La Niña events, rather than moderate events (Table 3). The variations in tornado occurrences based on ENSO intensity are analogous to tornado fatalities; more fatalities occurred during weak and strong El Niño and La Niña phases, rather than moderate phases (Table 3). However, weak and strong phases of El Niño and La Niña have occurred more frequently than moderate phases during the analysis temporal period (DJF 1953–2016; Table 3). Thus, the opportunities for tornadoes to occur during weak or strong ENSO phases as compared with moderate phases have simply been more numerous.

TABLE 1. The EF1+ and significant (EF2+) tornadoes and associated fatalities as occurrence percentages per season for the CONUS and SE-US from December 1953 through November 2016. Occurrence percentages (%) and raw numbers (No.) for tornado days and significant tornado days are also included.

|  | EF1+ (%), deaths (%) | EF2+ (%), deaths (%) | Tornado days (%, No.) | Significant tornado days (%, No.) |
|---|---|---|---|---|
| CONUS |  |  |  |  |
| DJF | 9.4, 14.2 | 10.4, 14.1 | 9.3, 1033 | 10.2, 437 |
| MAM | 44.5, 66.8 | 49.0, 68.0 | 31.2, 3456 | 38.9, 1658 |
| JJA | 31.7, 10.1 | 26.2, 9.3 | 41.4, 4593 | 35.2, 1502 |
| SON | 14.5, 8.9 | 14.4, 8.6 | 17.8, 1969 | 15.7, 668 |
| SE-US |  |  |  |  |
| DJF | 20.7, 24.5 | 23.3, 24.5 | 15.0, 706 | 23.0, 326 |
| MAM | 45.7, 61.8 | 49.2, 62.4 | 32.6, 1,535 | 42.9, 607 |
| JJA | 14.1, 1.9 | 8.8, 1.6 | 34.8, 1,641 | 14.8, 209 |
| SON | 19.5, 11.8 | 18.6, 11.6 | 17.4, 817 | 19.3, 273 |

### 1) GoM, ENSO, and winter tornadoes

Both ENSO and the GoM influence DJF significant tornado activity. The ≥90th percentile (%tile) of ranked significant tornado seasonal totals is characterized by Niño-3.4 region SSTA variance ≥ $6.0°C^2$ and mean GoM basin SSTAs ≥ 0.5°C as compared with climatology ($\alpha = 0.05$; Figs. 1a,b). SSTA variance in the Niño-3.4 region reflects strong El Niño and La Niña events. In contrast, the ≤10th %tile of ranked significant tornado seasonal totals is associated with little SSTA variance in the Niño-3.4 region and mixed/weak SSTAs in the GoM as compared with climatology, representative of ENSO-neutral conditions and a lack of a distinct GoM influence (Figs. 1c,d). Similar results can be appreciated in Niño-3.4 region SSTA variance for the ≤20th %tile of ranked EF1+ tornado seasonal totals for the CONUS and SE-US (Figs. 2c,g). Niño-3.4 region SSTA variance of $2.0°–5.0°C^2$ ($\alpha = 0.05$) is evident when analyzing the ≥80th %tile of ranked EF1+ tornado seasonal totals across the CONUS, illustrating that ENSO intensity plays a role in DJF tornado frequency (Fig. 2d). Positive mean GoM SSTAs are also distinguishable (+0.3°–0.5°C; nonsignificant), along with a new signal that emerges over the northeastern Pacific Ocean characterized by mean SSTAs ≤ −1.3°C ($\alpha = 0.05$; Fig. 2b). The northeastern

Pacific SSTA signal is likely driven by teleconnections to ENSO and tropical forcing (Alexander et al. 2002). Positive GoM SSTAs are present during the ≥80th %tile of ranked EF1+ tornado seasonal totals across the SE-US, particularly in the LC region, suggesting that northward LC protrusions increase DJF tornadic activity in proximal states ($\alpha = 0.05$; Fig. 2f). Positive SSTAs are also evident in the western Caribbean Sea, along with negative SSTAs in the northeastern Pacific Ocean ($\alpha = 0.05$; Fig. 2f). These signals suggest that SSTAs in the western Caribbean Sea and Gulf of Alaska occur much earlier than suggested by Elsner and Widen (2014), and also influence DJF tornado activity.

### 2) Winter variability of significant tornado environments

The influence of ENSO and the GoM on DJF significant tornado variability is also reflected in their joint modifications to significant tornado environments across certain geographical areas. In the Midwest and Midsouth, 50%–80% of the total frequency of mean STP 3-Hours have transpired during La Niña (Fig. 3d). In Florida and coastal South Carolina and Georgia, El Niño accounts for 60%–80% of the total frequency of mean STP 3-Hours (Fig. 3c). During ENSO-neutral

TABLE 2. DJF (1953–2016) EF1+ and significant (EF2+) tornadoes, fatalities, tornado days, and significant tornado days as occurrence percentages for the CONUS and SE-US during El Niño (ONI ≥ 0.5), La Niña (ONI ≤ −0.5), and ENSO-neutral (−0.5 < ONI < 0.5) conditions. DJF was used to calculate ONI. The frequencies of tornado days and significant tornado days are also included (No.). The ENSO count contains ENSO phase frequencies.

|  | EF1+ (%), deaths (%) | EF2+ (%), deaths (%) | Tornado days (%, No.) | Significant tornado days (%, No.) | ENSO count |
|---|---|---|---|---|---|
| El Niño CONUS | 32.7, 43.9 | 31.5, 44.5 | 35.4, 366 | 35.2, 154 | 23 |
| La Niña CONUS | 46.6, 50.0 | 49.3, 49.9 | 39.7, 410 | 43.2, 189 | 22 |
| ENSO-neutral CONUS | 20.7, 6.1 | 19.2, 5.7 | 24.9, 257 | 21.5, 94 | 18 |
| El Niño SE-US | 32.0, 43.0 | 31.6, 43.3 | 35.6, 251 | 36.8, 120 | 23 |
| La Niña SE-US | 47.5, 54.4 | 51.8, 54.5 | 41.9, 296 | 44.8, 146 | 22 |
| ENSO-neutral SE-US | 20.6, 2.6 | 16.6, 2.1 | 22.5, 159 | 18.4, 60 | 18 |

TABLE 3. DJF (1953–2016) EF1+ and significant (EF2+) tornadoes, fatalities, tornado days, and significant tornado days as occurrence percentages for the CONUS and SE-US during weak El Niño (0.5 ≤ ONI < 1.0) and La Niña (−1.0 < ONI ≤ −0.5), moderate El Niño (1.0 ≤ ONI < 1.5) and La Niña (−1.5 < ONI ≤ −1.0), and strong El Niño (ONI ≥ 1.5) and La Niña (ONI ≤ −1.5) phases. Tornado days and significant tornado days frequencies are also included (No.). ENSO count contains ENSO phase frequencies.

| | EF1+ (%), deaths (%) | EF2+ (%), deaths (%) | Tornado days (%, No.) | Significant tornado days (%, No.) | ENSO count |
|---|---|---|---|---|---|
| Weak El Niño CONUS | 13.1, 20.1 | 12.2, 19.9 | 16.6, 171 | 15.1, 66 | 12 |
| Weak La Niña CONUS | 22.1, 11.7 | 24.1, 11.3 | 20.5, 212 | 22.0, 96 | 12 |
| Weak El Niño SE-US | 14.4, 18.1 | 13.6, 18.0 | 17.0, 120 | 17.2, 56 | 12 |
| Weak La Niña SE-US | 23.8, 11.9 | 27.6, 11.6 | 22.4, 158 | 25.2, 82 | 12 |
| Moderate El Niño CONUS | 3.1, 6.9 | 3.5, 7.3 | 3.8, 39 | 4.6, 20 | 4 |
| Moderate La Niña CONUS | 7.6, 21.6 | 9.1, 22.1 | 6.0, 62 | 7.8, 34 | 4 |
| Moderate El Niño SE-US | 2.8, 9.1 | 3.6, 9.5 | 3.5, 25 | 4.3, 14 | 4 |
| Moderate La Niña SE-US | 5.8, 25.6 | 7.4, 26.1 | 6.4, 45 | 7.1, 23 | 4 |
| Strong El Niño CONUS | 16.5, 16.9 | 15.8, 17.3 | 15.1, 156 | 15.6, 68 | 7 |
| Strong La Niña CONUS | 17.0, 16.7 | 16.1, 16.4 | 13.2, 136 | 13.5, 59 | 6 |
| Strong El Niño SE-US | 14.7, 15.7 | 14.4, 15.9 | 15.0, 106 | 15.3, 50 | 7 |
| Strong La Niña SE-US | 17.8, 17.0 | 16.8, 16.8 | 13.2, 93 | 12.6, 41 | 6 |

conditions, lower occurrences of significant tornadoes are substantiated by less frequent significant tornado environments (Fig. 3b). Nevertheless, warm (cold) GoM SSTs can increase (decrease) the occurrence of environments favorable for tornadic activity during El Niño, La Niña, and ENSO-neutral years. The ≥75th %tile of GoM basin SSTAs account for 40%–80% of mean STP 3-Hours across the Great Plains and Midwest, and the ≤25th %tile result in 10%–40% across the Great Plains and southern CONUS (Figs. 4a,b). The ≥75th %tile of GoM LC region SSTAs account for 30%–40% of total mean STP 3-Hours across the Florida Peninsula (Fig. 4d), an anomaly absent during the ≤25th %tile SSTAs (Fig. 4c). Variability of the GoM WCR region in relation to mean STP 3-Hours suggests that the western GoM can have far-reaching effects; the ≥75th %tile of GoM WCR region SSTAs account for 40%–70% mean STP 3-Hours across the Great Plains and Midwest (Fig. 4f).

Significant tornado environment modulations by ENSO and the GoM are also evident in the daily probabilities of mean STP 3-Hours ≥ 1. Climatology shows that the DJF daily probability of mean STP 3-Hours ≥ 1 peaks at 1%–2% across southeastern Texas and southern Louisiana (Fig. 3a). When considering the ≥80th %tile of GoM basin SSTAs during all study years (1981–2016), the daily probability of mean STP 3-Hours ≥ 1 increases from northeastern Texas to the Midsouth (α = 0.05; Fig. 5b). In contrast, the ≤20th %tile of GoM basin SSTAs result in a decrease in the daily probability of mean STP 3-Hours ≥ 1 across the Midsouth (α = 0.05; Fig. 5a). In the absence of El Niño or La Niña, the GoM can contribute to a decrease in significant tornado environments when anomalously cool. The ≤30th %tile of GoM basin SSTAs during ENSO-neutral years show that the daily probability of mean STP 3-Hours ≥ 1 decreases

across parts of the SE-US relative to ENSO-neutral climatology (α = 0.05) %tile (Fig. 5c). GoM contributions to a favorable significant tornado environment are physically reasonable; a warmer (cooler) GoM results in more (less) moisture available for advection toward the CONUS, leading to increased (decreased) convective and tornadic activity potential. These results support the GoM as a source of climate variability of DJF significant tornadoes in conjunction with, and independent of, ENSO.

### 3) ENSO TORNADO ACTIVITY VARIES WITH ONI MAGNITUDE

ENSO-based intensity modulations are apparent in the significant tornado environment during DJF. Overall, stronger ENSO phases lead to increases in the daily probability of mean STP 3-Hours ≥ 1 (Figs. 5f,h). During the ≥75th %tile of El Niño DJFs ranked by ONI, an increase in the daily probability of mean STP 3-Hours ≥ 1 occurs from eastern Texas to the Midsouth relative to the climatology of El Niño events (α = 0.05; Fig. 5f). Moderate-to-strong El Niño events also favor occurrences of mean STP 3-Hours ≥ 1 across Florida (Figs. 3e and 5f). The ≤25th %tile of El Niño DJFs ranked by ONI results in a decrease in the daily probability of mean STP 3-Hours ≥ 1 across the southern CONUS, albeit a nonsignificant one (Fig. 5e). During the ≥75th %tile of La Niña DJFs ranked by |ONI|, an increase in the daily probability of mean STP 3-Hours ≥ 1 occurs across central Texas and western Tennessee relative to the climatology of La Niña events (α = 0.05; Fig. 5h). Moderate-to-strong La Niña events do not favor significant tornado environments across the eastern SE-US, as is evident in the absence of mean STP 3-Hours from the Florida Peninsula to the South Carolina coast (Fig. 3f).
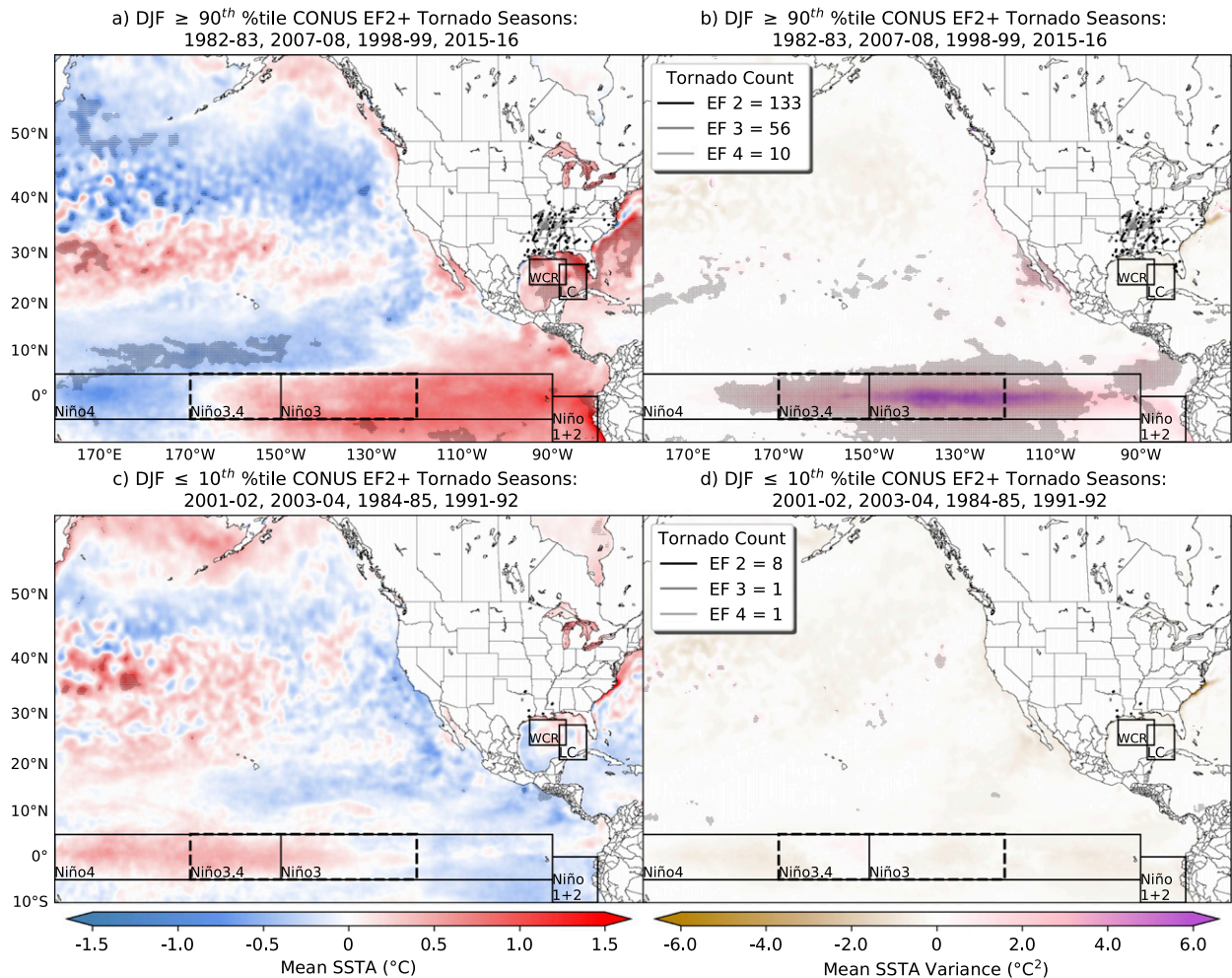
FIG. 1. SSTA mean and variance from DJF (1981–2016) climatology during the (a),(b) ≥90th %tile and (c),(d) ≤10th %tile of ranked significant (EF2+) tornado seasonal totals for the CONUS, with tornado paths as indicated in the legend. Two-tailed statistical significance ($\alpha = 0.05$), determined using a 20 000-member Monte Carlo distribution of bootstrap anomalies from climatology, is indicated with stippling. Polygons demarcate SST areas of interest and include Niño-4, Niño-3.4 (dashed), Niño- 3, Niño-1+2, and GoM LC and WCR regions.

Variability of significant tornado environments due to ENSO magnitude could be related to jet stream modulations, as demonstrated by Cook et al. (2017) for baseline El Niño and La Niña events. These results show that while both El Niño and La Niña are related to increases in significant tornado environments, there is greater variance in increased significant tornado environments during strong El Niño events as compared with strong La Niña events. Note that composites of only El Niño or La Niña years result in small sample sizes that can be sensitive to individual tornado events, particularly during DJF, when there is a propensity for tornado events to be driven by midlatitude systems.

### b. Winter subseasonal tornado variability

Intraseasonal variability in DJF tornado frequency is apparent during strong ENSO phases. For instance,

during the strong 1998–99 La Niña, 46 of 51 significant DJF tornadoes occurred during the month of January, with 0 and 5 in December and February, respectively (Fig. 6). Intraseasonal variability in DJF tornado frequency is also evident in conjunction with positive GoM SSTAs. The Decembers of 1986 and 1998 had GoM SSTAs ≥ 0.4°C, but they were below their monthly significant tornado total mean (Fig. 7b). We identify potential reasons for DJF intraseasonal tornado variability in relation to ENSO and the GoM in the subsections that follow.

### 1) EL NIÑO EARLIER, LA NIÑA LATER

Despite the persistence of the ENSO signal on the seasonal time scale, intraseasonal variability exists in DJF tornado frequency. Subseasonal analysis reveals that significant tornado occurrence is favored in December
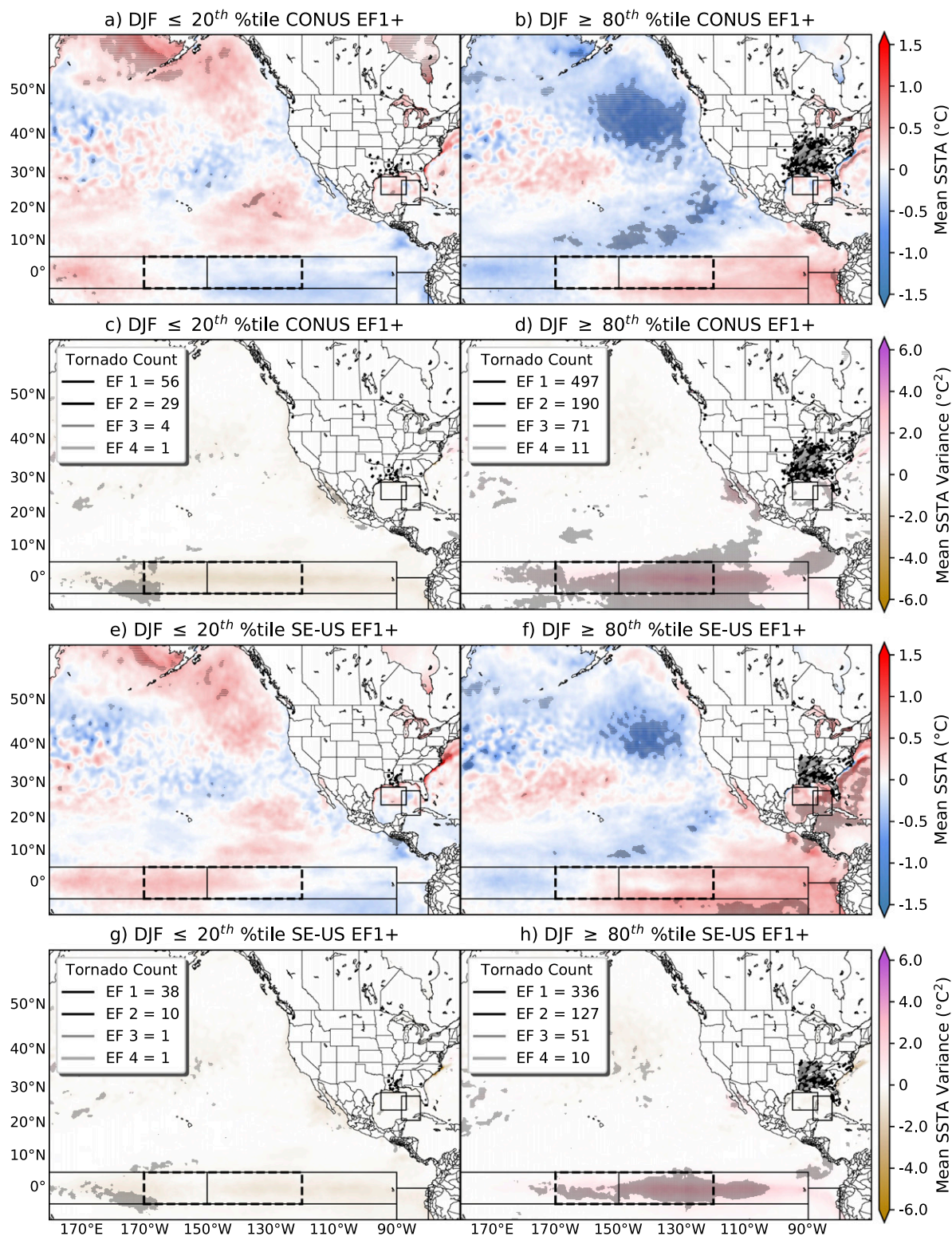
FIG. 2. As in Fig. 1, but during the (left) ≤20th %tile and (right) ≥80th %tile of ranked EF1+ tornado seasonal totals across the (a)–(d) CONUS and (e)–(h) SE-US. SST areas of interest are demarcated by polygons, as labeled in Fig. 1.
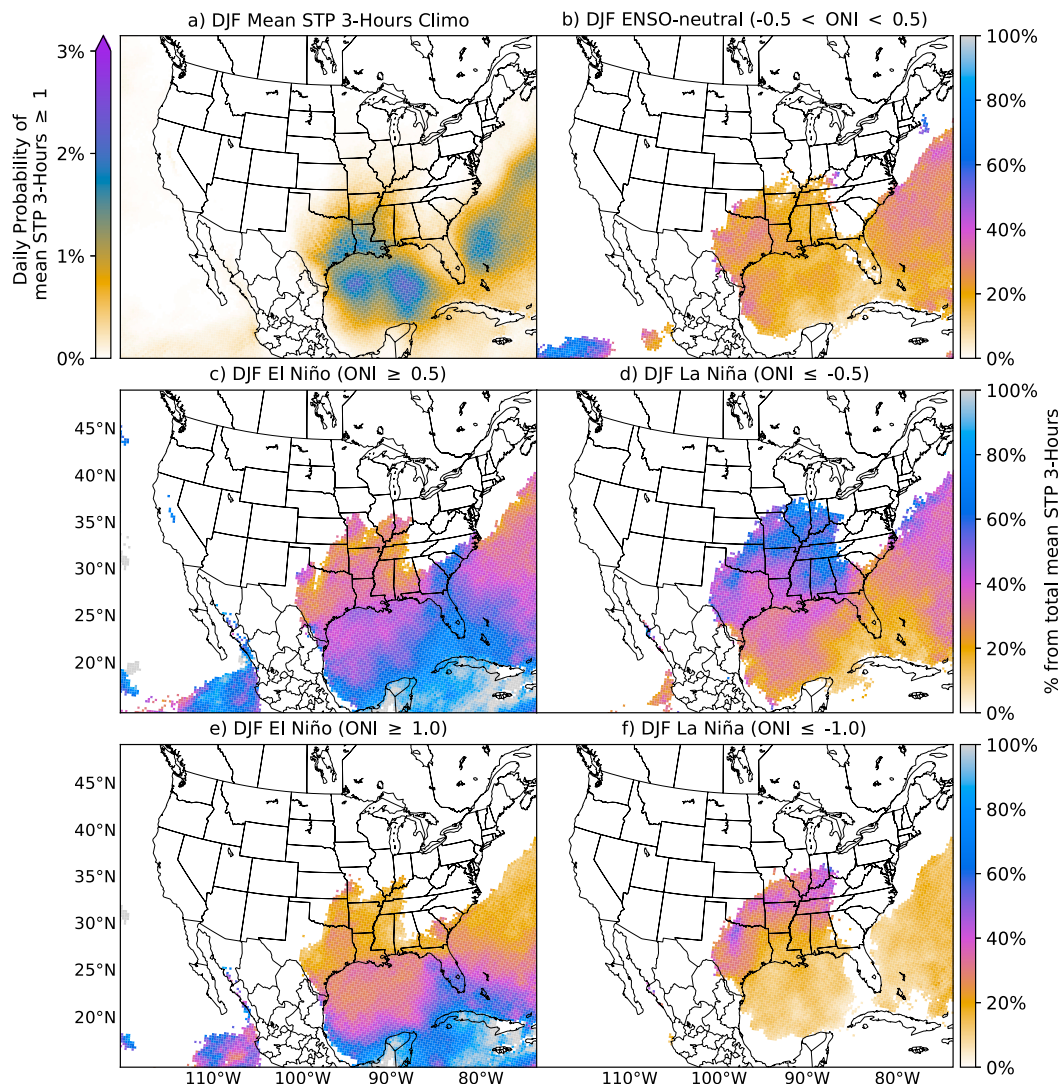
FIG. 3. DJF (1981–2016) climatologies of mean STP 3-Hours, including (a) daily probability of ≥1 and percent of total during (b) ENSO-neutral, (c) El Niño, (d) La Niña, (e) moderate-to-strong El Niño, and (f) moderate-to-strong La Niña conditions.

during El Niño (Figs. 6b and 7b), and favored in January and February during La Niña (Figs. 6c,d and 7c,d), as shown in Allen et al. (2018). For instance, during the strong 1982–83 El Niño, 37 significant tornadoes occurred in December, while 2 occurred in January (Fig. 6). In contrast, most ENSO-neutral phases remain below the respective monthly significant tornado count mean (Figs. 6b–d). Subseasonal variability in relation to ENSO can also be appreciated in EF1+ tornado totals. El Niño EF1+ tornadoes (Table 4, top) are more frequent in December, while La Niña EF1+ tornadoes are more frequent in January (Table 4, middle) and February (Table 4, bottom).

ENSO-related subseasonal tornado variability is also reflected in significant tornado environments. A southward

progression in positive anomalies of the daily probability of mean STP 3-Hours ≥ 1 occurs from December through February during the ≥75th %tile of El Niño events ranked by ONI, encompassing eastern Texas to the Midwest in December, southeastern Texas in January, and Florida in February ($\alpha = 0.05$; Figs. 8f, 9f, and 10f). The southward migration of positive significant tornado environment anomalies during stronger El Niño events may be related to an enhanced subtropical jet, associated with a strengthening of the Hadley cell by tropical Pacific convection (Montroy 1997; Barlow et al. 2001). Note that positive anomalies of the daily probability of mean STP 3-Hours ≥ 1 in December coincide with GoM SSTAs ≥ 1.0°C across the basin (not shown), and thus the significant tornado
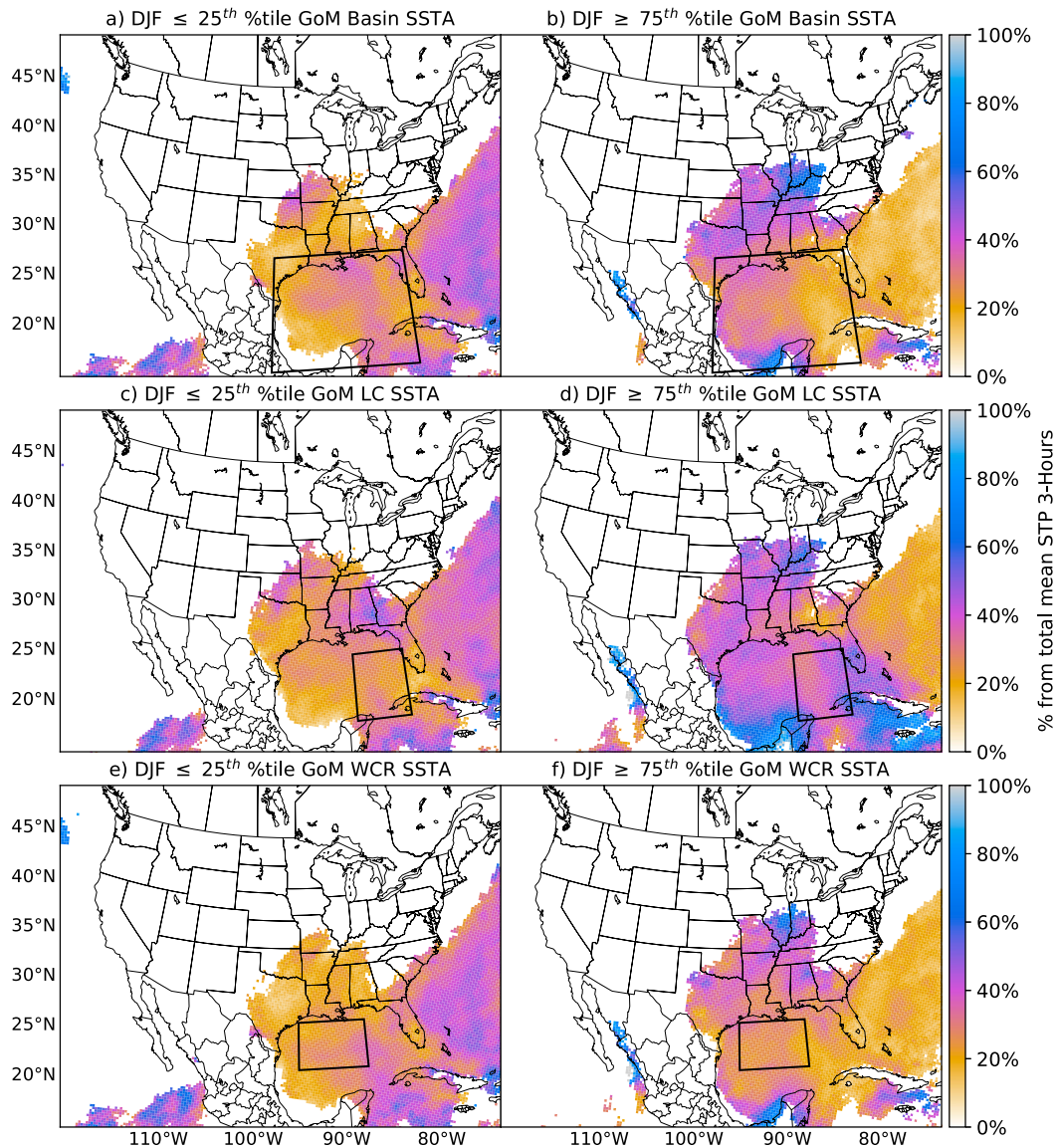
FIG. 4. DJF (1981–2016) percent of total mean STP 3-Hours during the (left) ≤25th %tile and (right) ≥75th %tile of the (a),(b) GoM basin, (c),(d) GoM LC region, and (e),(f) GoM WCR region SSTAs. Polygons indicate SSTA regions.

environment may also be due in part to increased CAPE and low-level moisture from the GoM.

Variability in the daily probability of a favorable significant tornado environment is also evident during La Niña (Figs. 8g,h, 9g,h, and 10g,h). Overall, the ≥75th %tile of La Niña events ranked by |ONI| lead to positive anomalies of the daily probability of mean STP 3-Hours ≥ 1 as follows: across central Texas in December, from northeastern Texas to the Midwest in January, and across east Texas and the Midsouth in February (Figs. 8h, 9h, and 10h). These variations in environments based on La Niña intensity are physically

plausible. Pacific anticyclones could be more intense during stronger La Niña events, resulting in an increased meridional nature of the polar jet stream downstream of the tropical Pacific and thus more favorable tornado environments across the CONUS (Allen et al. 2015; Cook et al. 2017). Of interest, the ≥75th %tile of La Niña events ranked by |ONI| also result in a decrease in the daily probabilities of mean STP 3-Hours ≥ 1 along the Gulf Coast in January (nonsignificant; Fig. 9h), despite the presence of positive GoM SSTAs ≥ 1°C (not shown). This result suggests that northward polar jet stream shifts during La Niña can result in a less
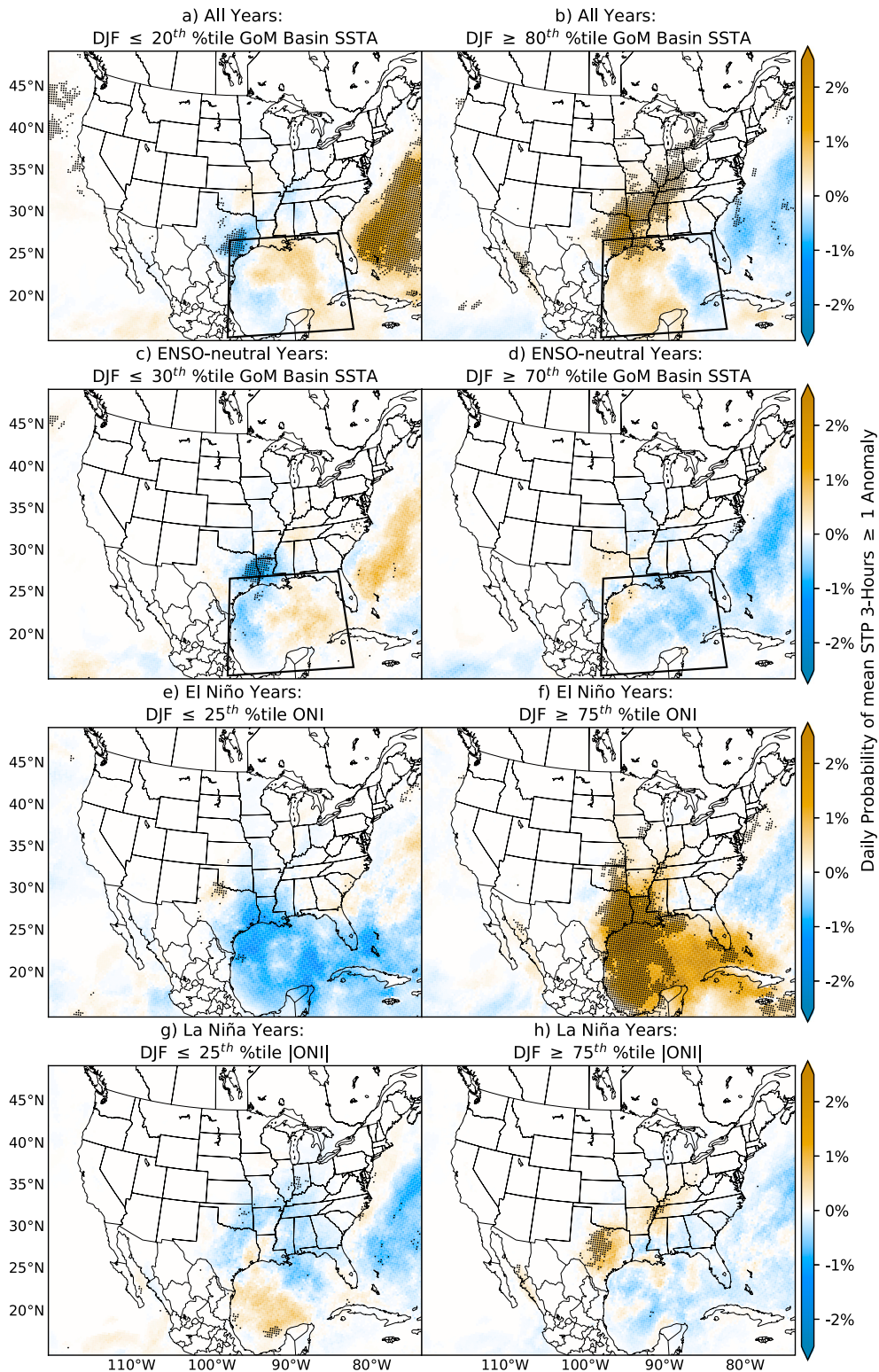
FIG. 5. DJF (1981–2016) daily probability of mean STP 3-Hours ≥ 1 anomalies for (a),(b) ≤20th %tile (cold) and ≥80th %tile (warm) of ranked SSTAs for the GoM basin (polygon indicated), (c),(d) ≤30th %tile (cold) and ≥70th %tile (warm) of ranked SSTAs for the GoM basin during ENSO-neutral years, (e),(f) ≤25th %tile (weaker) and ≥75th %tile (stronger) of El Niño ranked by ONI, and (g),(h) ≤25th %tile (weaker) and ≥75th %tile (stronger) of La Niña ranked by |ONI|. Significance ($\alpha$ = 0.05) is as in Fig. 1.
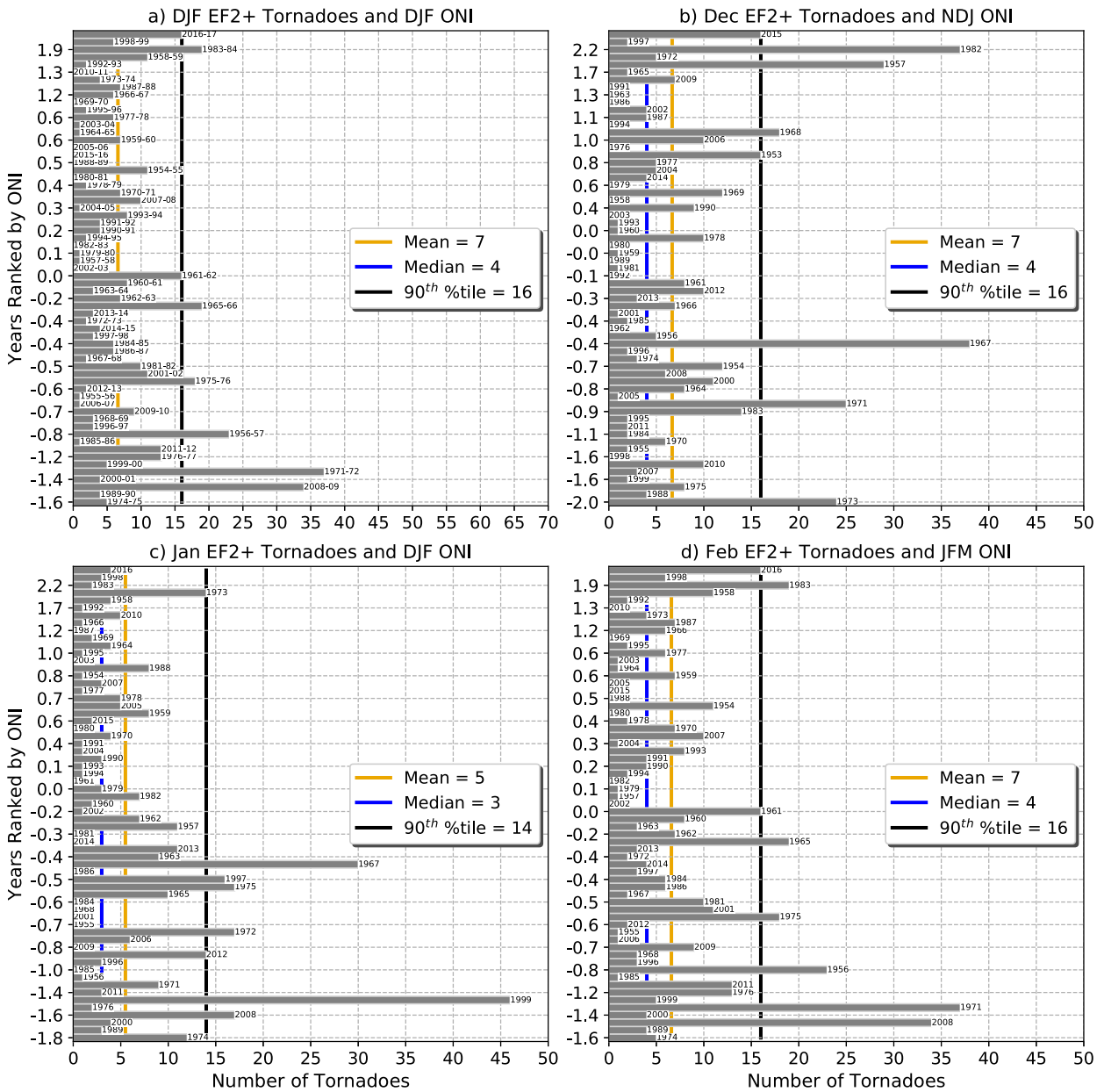
FIG. 6. DJF (1953–2016) significant (EF2+) tornadoes for the CONUS ranked by (a) DJF ONI for DJF, (b) NDJ ONI for December, (c) DJF ONI for January, and (d) JFM ONI for February. Mean, median, and 90th %tile of tornado count distribution are indicated in the legend.

favorable kinematic vertical profile for tornadoes near Gulf Coast regions. It is important to note that the study sample size is reduced substantially when considering intensity-stratified El Niño or La Niña years and care not to overinterpret results should be taken because of the resulting uncertainty.

### 2) SUBSEASONAL TORNADO VARIABILITY DRIVEN BY THE GoM AND ENSO

GoM SSTs can result in modulations to subseasonal tornado frequency and significant tornado environments

in conjunction with ENSO (Figs. 8a,b, 9a,b, and 10a,b). During the ≥80th %tile of GoM basin SSTAs, an increase occurs in the daily probability of mean STP 3-Hours ≥ 1 across the SE-US in December months of all study years ($\alpha = 0.05$; Fig. 8b). In February months of all study years, the ≥80th %tile (≤20th %tile) of GoM basin SSTAs is associated with an increase (decrease) in the daily probability of mean STP 3-Hours ≥ 1 across southeastern Texas and Louisiana (from Louisiana to the Florida Panhandle (both $\alpha = 0.05$; Figs. 10a,b). Signals are weaker/mixed during the ≤20th %tile of
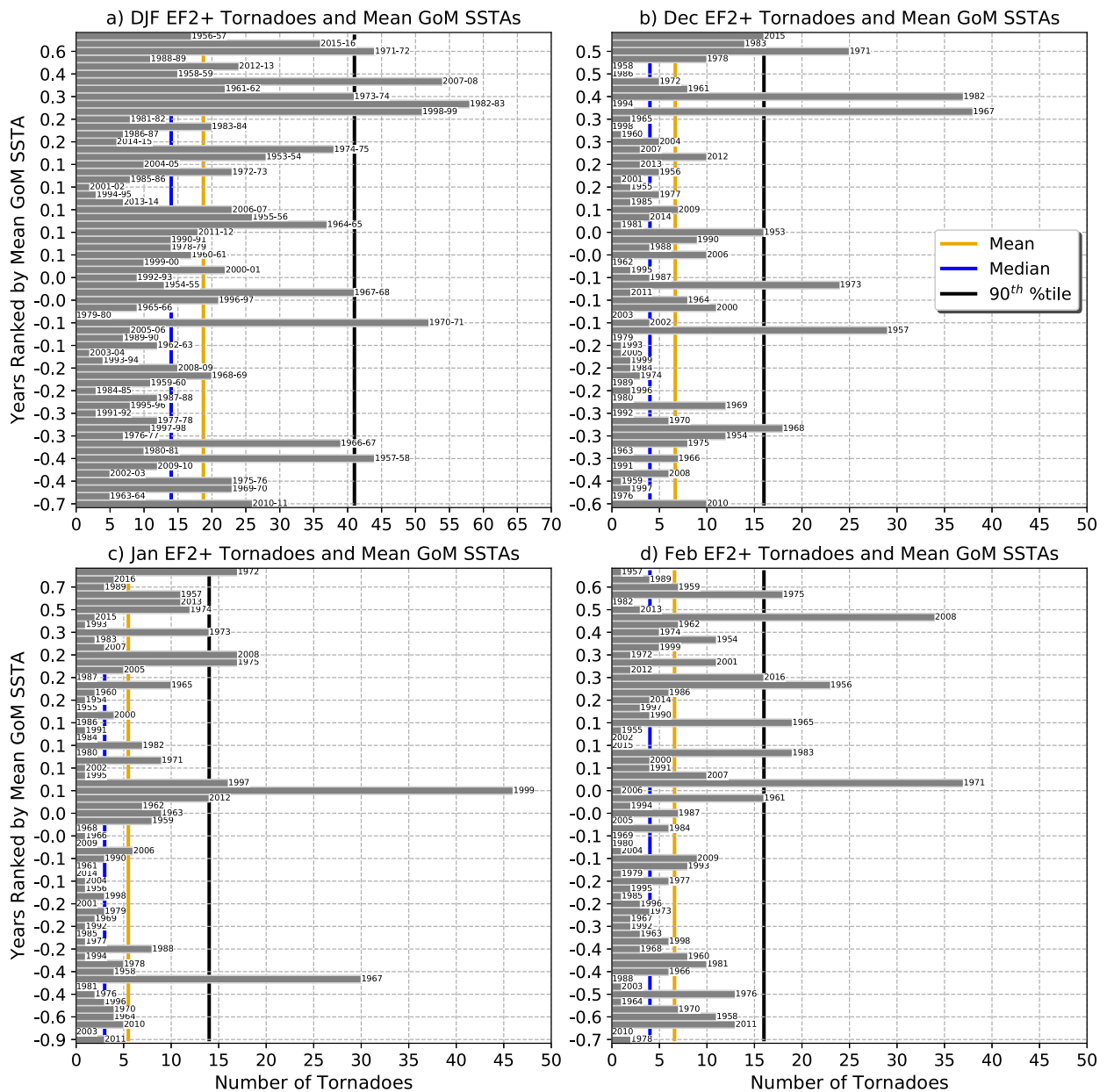
FIG. 7. DJF (1953–2016) significant (EF2+) tornadoes for the CONUS ranked by area-averaged GoM basin SSTA for (a) DJF, (b) December, (c) January, and (d) February. The legend is as in Fig. 6.

GoM basin SSTAs in December and January of all study years, likely because of the influence of ENSO and/or other known, or unknown, sources of climate variability (Figs. 8a and 9a,b).

During ENSO-neutral DJF months, the GoM can enhance or diminish the environment favorable for significant tornadoes. In December months concurrent to ENSO-neutral conditions, the ≥70th %tile and ≤30th %tile of GoM basin SSTAs reveal anomalies in the daily probability of mean STP 3-Hours ≥ 1 similar

to the signal during all study years, albeit nonsignificant (Figs. 8c,d). These results suggest that the GoM can provide a source of predictability for subseasonal tornadic environments in December months when ENSO is neutral. During ENSO-neutral January and February months, the influence of GoM SSTAs on the significant tornado environment is mixed (Figs. 9c,d and 10c,d), suggesting that another known or unknown climate oscillation may play a role in tornado occurrence, or that a local source of moisture (e.g., early snowmelt) could be

TABLE 4. As in Table 2, but for the months of December, January, and February from December 1953 through February 2016. ONI was calculated using NDJ for December, DJF for January, and JFM for February.

| | EF1+ (%), deaths (%) | EF2+ (%), deaths (%) | Tornado days (%, No.) | Significant tornado days (%, No.) | ENSO count |
|---|---|---|---|---|---|
| | | | December | | |
| El Niño CONUS | 41.1, 66.7 | 41.9, 69.2 | 37.7, 123 | 42.1, 64 | 23 |
| La Niña CONUS | 34.9, 22.4 | 34.5, 19.8 | 33.4, 109 | 35.5, 54 | 20 |
| ENSO-neutral CONUS | 24.0, 10.9 | 23.6, 11.0 | 28.8, 94 | 22.4, 34 | 20 |
| El Niño SE-US | 37.0, 64.5 | 37.4, 65.7 | 40.7, 90 | 43.0, 49 | 23 |
| La Niña SE-US | 37.9, 23.6 | 38.1, 23.1 | 33.0, 73 | 35.1, 40 | 20 |
| ENSO-neutral SE-US | 25.1, 11.8 | 24.5, 11.1 | 26.2, 58 | 21.9, 25 | 20 |
| | | | January | | |
| El Niño CONUS | 26.6, 45.3 | 22.5, 46.4 | 35.3, 117 | 34.9, 44 | 23 |
| La Niña CONUS | 52.0, 36.7 | 52.0, 35.2 | 40.8, 135 | 41.3, 52 | 22 |
| ENSO-neutral CONUS | 21.3, 18.0 | 25.4, 18.4 | 23.9, 79 | 23.8, 30 | 18 |
| El Niño SE-US | 27.3, 55.7 | 25.8, 57.4 | 33.6, 77 | 36.6, 34 | 23 |
| La Niña SE-US | 54.7, 40.6 | 57.1, 39.4 | 44.5, 102 | 43.0, 40 | 22 |
| ENSO-neutral SE-US | 18.1, 3.8 | 17.2, 3.2 | 23.8, 50 | 20.4, 19 | 18 |
| | | | February | | |
| El Niño CONUS | 24.1, 26.4 | 21.2, 26.0 | 25.5, 96 | 20.8, 33 | 18 |
| La Niña CONUS | 43.8, 65.3 | 47.5, 66.2 | 35.4, 133 | 39.6, 63 | 19 |
| ENSO-neutral CONUS | 32.1, 8.3 | 31.3, 7.8 | 39.1, 147 | 39.6, 63 | 26 |
| El Niño SE-US | 25.4, 24.1 | 23.4, 23.8 | 24.2, 62 | 21.9, 26 | 18 |
| La Niña SE-US | 42.3, 67.3 | 46.5, 67.6 | 38.3, 98 | 41.2, 49 | 19 |
| ENSO-neutral SE-US | 32.3, 8.6 | 30.1, 8.6 | 37.5, 96 | 37.0, 44 | 26 |

enhancing low-level buoyancy, thus providing a more favorable thermodynamic environment. Such hypotheses raise interesting questions to be explored in future research, as they are beyond the scope of the present study. However, the limited sample size associated with analyzing only ENSO-neutral years could lead to individual seasons dominating the overall signal, presenting a difficult challenge to overcome given the limited temporal range of current higher-resolution reanalysis datasets.

The influence of ENSO and the GoM on significant tornado environment modulations is also apparent in tornado observations. Most high-frequency EF1+ tornado DJF months occurred during moderate-to-strong ENSO phases (Figs. 11a,c,e). Most high-frequency EF1+ tornado December and January months also had positive GoM SSTAs (Figs. 11b,d). Of interest is that relatively large EF1+ tornado counts have occurred in February with both positive and negative GoM SSTAs (Fig. 11f), reiterating that an alternate predictor could be playing a role in February tornado activity. Admittedly, some of the signals observed in EF1+ tornado and significant tornado environment variability could be only partly driven by ENSO and/or the GoM. It is notable that ENSO and ENSO-neutral phases have occurred in conjunction with positive and negative GoM basin SSTAs. Therefore, despite the tendency for GoM cooling (warming) during El Niño (La Niña), GoM basin SSTA variability can deviate from the influence of ENSO in DJF, as

found for MAM by Molina et al. (2016). Furthermore, both El Niño and La Niña can generate above-average DJF tornado activity across the CONUS, with La Niña generally producing greater tornado frequency than El Niño.

### c. Study sensitivity to seasonal classification

Results from this study show that ENSO-neutral phases are related to lower DJF tornado frequencies, but Cook and Schaefer (2008) and Cook et al. (2017) found that ENSO-neutral phases resulted in more frequent and greater magnitude CONUS winter tornado outbreaks. Discrepancies in study methods are the contributing factors to the disparities between the results herein and the results of Cook and Schaefer (2008) and Cook et al. (2017). Cook and Schaefer (2008) and Cook et al. (2017) focused on the variability of tornado "outbreak" days, classified as days in which six or more tornadoes occurred from 1950 through 2003 [derived in part from Pautz (1969)], providing justification that teleconnections with ENSO would be more readily observed on synoptic scales rather than the mesoscale (e.g., individual tornado events). Both studies also considered "strong and violent" tornado days, which were defined as a day with five or more significant tornadoes (Cook and Schaefer 2008; Cook et al. 2017). While tornado outbreak days and strong and violent tornado days are less sensitive to underreporting biases, such filtering can lead to the omission
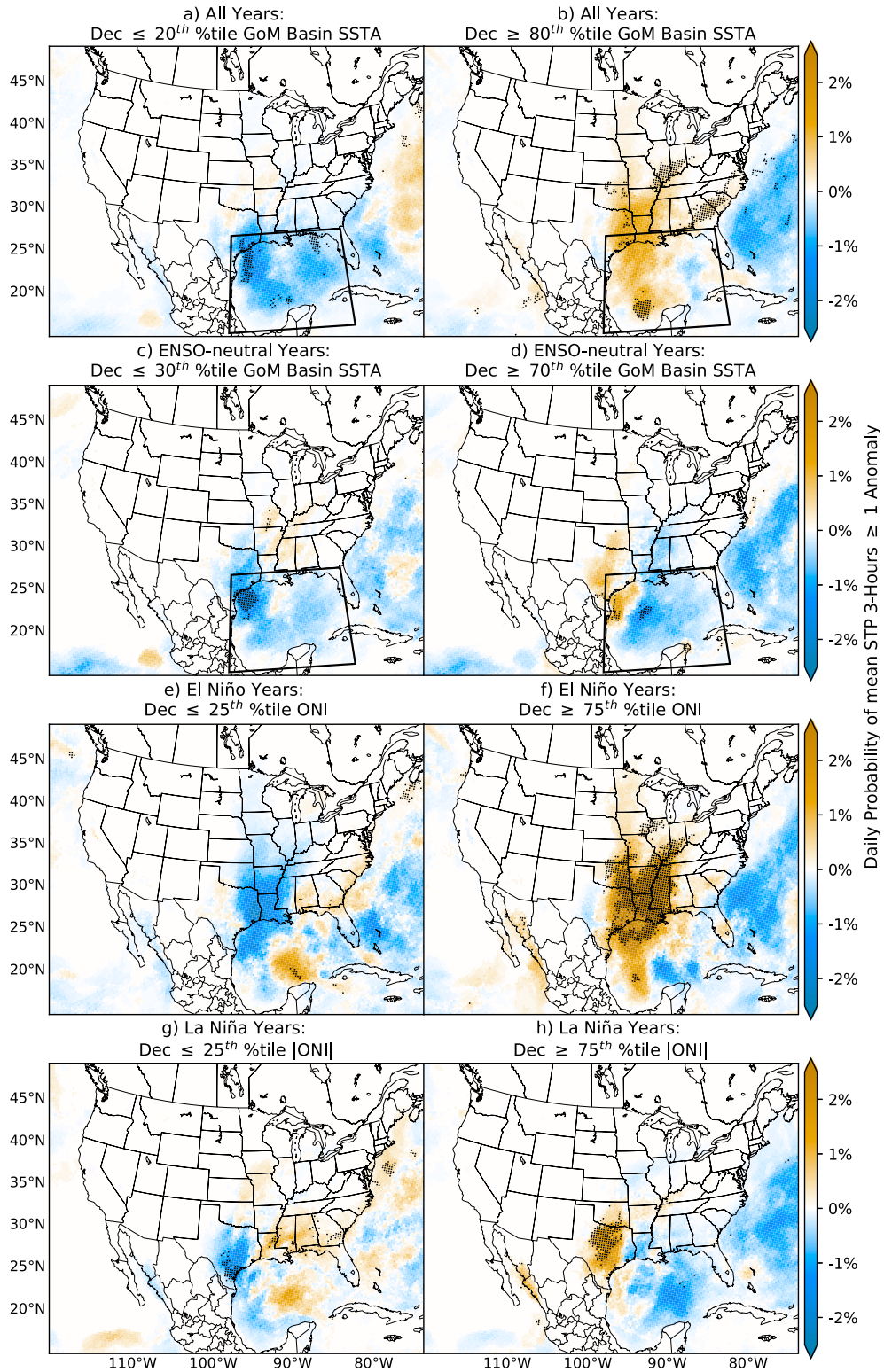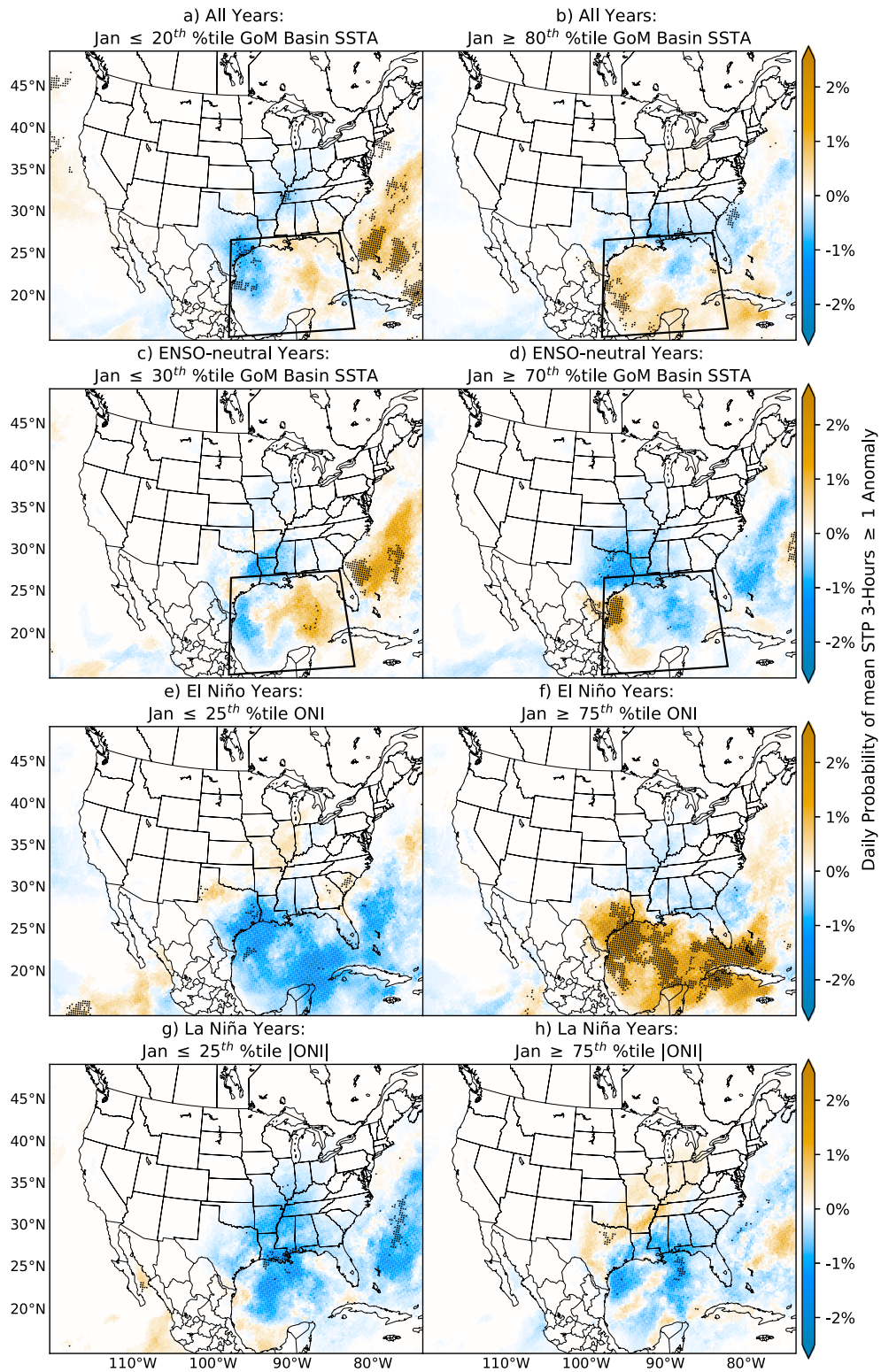
FIG. 8. As in Fig. 5, but for December.

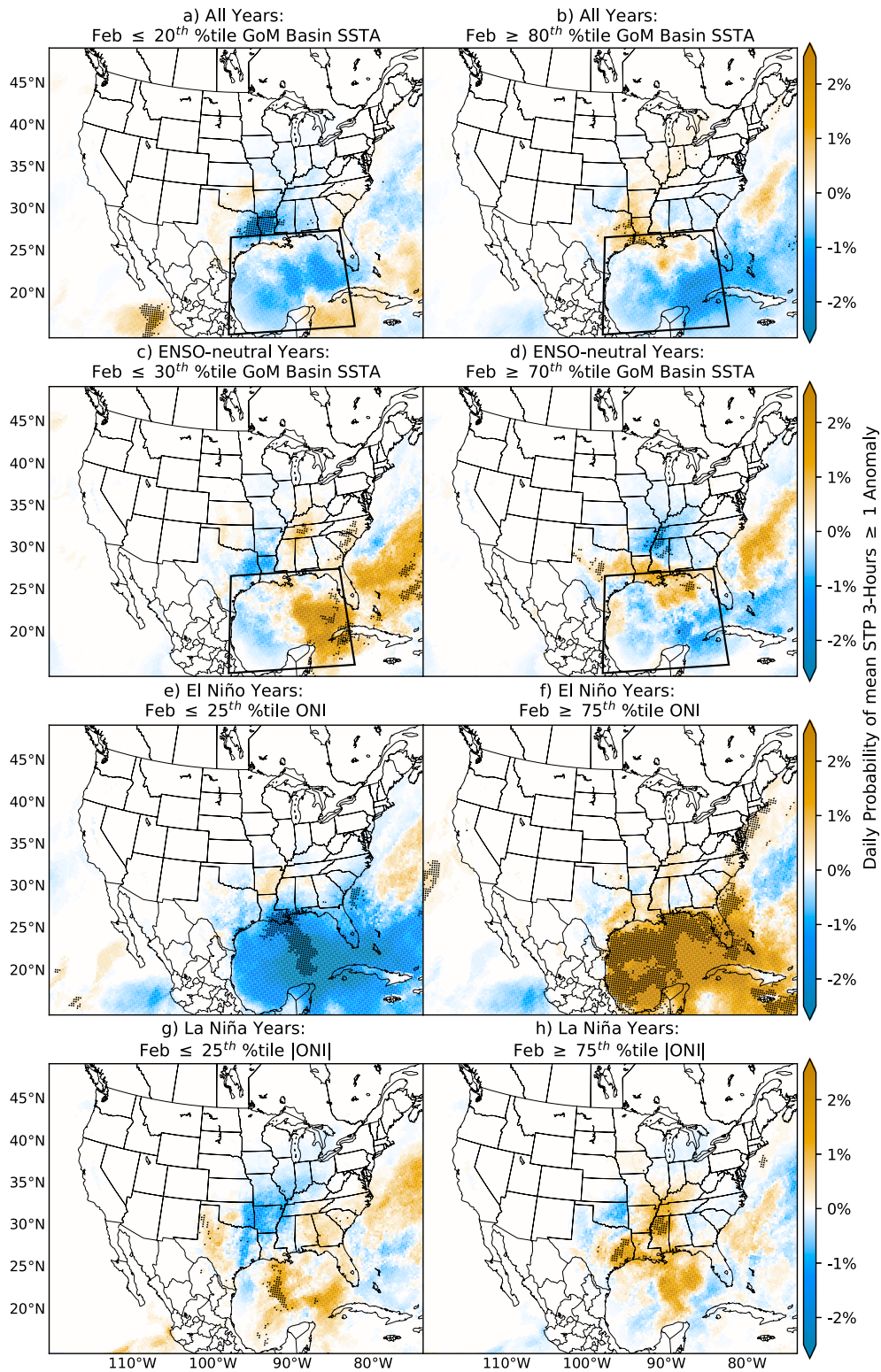FIG. 9. As in Fig. 5, but for January.
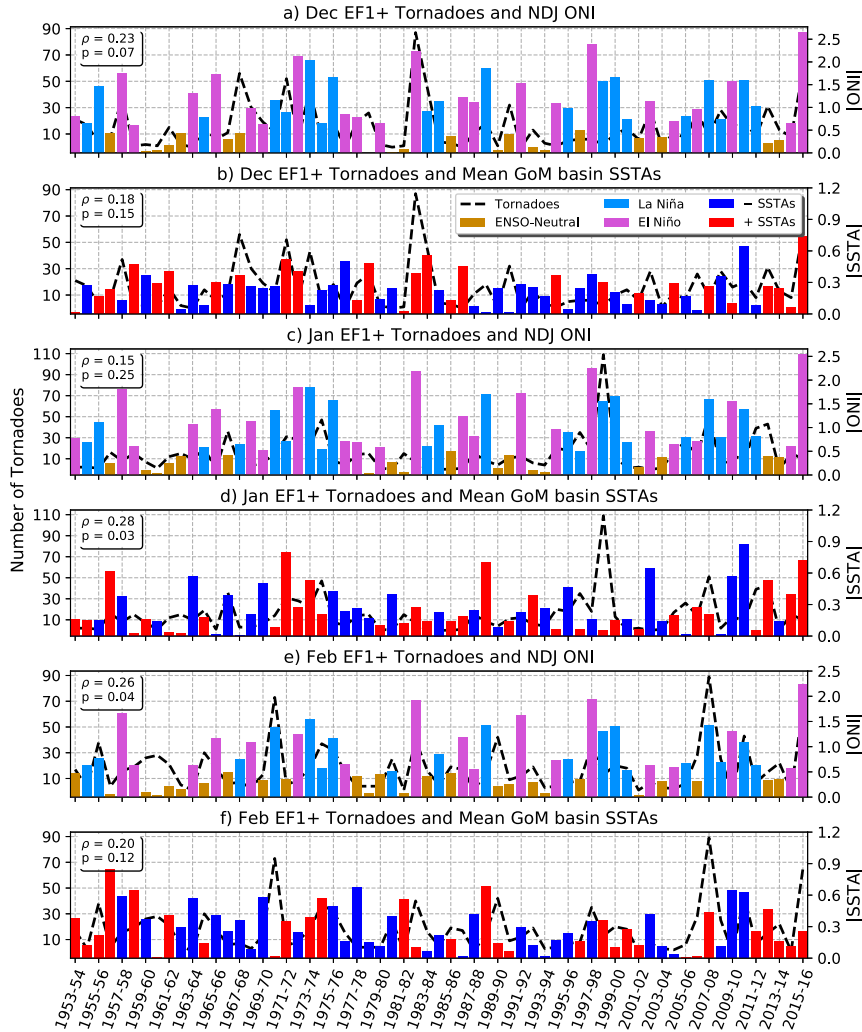
FIG. 10. As in Fig. 5, but for February.

FIG. 11. DJF (1953–2016) EF1+ tornadoes for the CONUS with absolute magnitude of (a),(c),(e) ONI and (b),(d),(f) area-averaged GoM basin SSTAs, as indicated in the legend. Spearman rank-order correlation coefficients and two-sided *p* values are shown in the legend.

of a considerable number of nontornado outbreak events and reduces a sample already limited by the seasonal cycle. For instance, 1033 tornado days contrast 220 tornado outbreak days during DJF from 1953 through 2016, which results in the omission of ~78% of DJF tornado days from analyses. A similar reduction in sample size can be appreciated when considering significant tornado days and outbreaks; 437 significant tornado days contrast 51 strong and violent tornado days during DJF from 1953 through 2016.

The temporal classification of winter also differs between studies. Cook and Schaefer (2008) and Cook et al. (2017) classified winter using the months of January–March (JFM). However, the peak amplitude of ENSO is usually during DJF, with a decay in intensity typically occurring during MAM (Trenberth 1997). The inclusion

of the month of March and omission of December increases the sample of ENSO-neutral years and decreases the sample of El Niño and La Niña years, whether classifying ENSO using ONI as in Cook and Schaefer (2008) or monthly Niño-3.4 region SSTAs as in Cook et al. (2017). For instance, using ONI to classify El Niño and La Niña, DJF is associated with 18 ENSO-neutral phases and 45 ENSO phases, while JFM is associated with 26 ENSO-neutral phases and 37 ENSO phases. To further illustrate this point, we bin DJF and JFM (1953–2016) tornado outbreak days and compute the percentage of tornado outbreak days occurring during ENSO-neutral phases for both. During ENSO-neutral phases of DJF 18.6% tornado outbreak days occurred, contrasting with 38.6% during ENSO-neutral

phases of JFM. The purpose of this section is not to dispute the methodological reasoning of Cook and Schaefer (2008) and Cook et al. (2017), as both studies provided justifiable experiment designs, but rather to highlight the result sensitivity in tornado variability studies that is associated with the months chosen to compose a season and the binning method of choice for tornado occurrences.

### d. Outlier cases of variability: Winter tornadoes of 1988–89 and 1997–98

ENSO is characterized by considerable internal variability, and as such, strong ENSO phases and warm GoM SSTs do not always result in large totals of DJF significant tornadoes. For instance, the 1988–89 La Niña resulted in a below-average DJF total of 11 significant tornadoes yet is the strongest La Niña on record since December 1981. GoM basin SSTAs for DJF were also positive, but characterized by substantial intraseasonal variability. There is a tendency for anticyclonic flow across the Gulf of Alaska region during La Niña events, which can steer the polar jet stream northward and lead to an increasingly meridional flow downstream, as illustrated in Figs. 12e,f with mean La Niña events of 1979–2016 (13 total La Niña events). Thus, La Niña can lead to increased cyclogenesis on the lee of the Rockies and farther north advection of GoM moisture, a favorable climatological base state for active DJF tornado seasons (Allen et al. 2015; Cook et al. 2017). However, the 1988–89 La Niña occurred in conjunction with a stronger northeastern Pacific anticyclone with far north latitudinal extent (nonsignificant; Fig. 12b) as compared with mean La Niña events (Fig. 12f). The northward latitudinal shift in the anticyclone position created unfavorable jet dynamics for CONUS severe thunderstorms (Figs. 12a,b). In fact, 500-hPa geopotential height anomalies indicate ridging across the SE-US, with anomalous troughing positioned farther north across eastern Canada ($\alpha = 0.05$; Fig. 12b). The 1988–89 La Niña demonstrates that there is greater variance in the covaried La Niña teleconnections, which can create or diminish favorable seasonal and subseasonal tornado environments. These results suggest that potential exists during strong La Niña events to provide a challenging degree of difficulty for seasonal forecasting of tornado activity, consistent with the results of Allen et al. (2015).

Variance also exists within El Niño events. The 1997–98 El Niño is the second strongest on record since December of 1981, yet resulted in below-average monthly totals of significant tornadoes across the CONUS. However, mean GoM basin SSTAs were below average ($\sim -0.3°C$) during DJF 1997–98, perhaps limiting low-level moisture return. El Niño typically

occurs in conjunction with cyclonic flow across the Gulf of Alaska, as illustrated with mean El Niño events of 1979–2016 in Figs. 12g,h (13 total El Niño events). El Niño can result in the subtropical jet stream positioned across the southern CONUS, yielding favorable kinematic vertical profiles for tornadic activity along Gulf Coast states (Allen et al. 2015; Cook et al. 2017). However, during the strong 1997–98 El Niño, the Gulf of Alaska cyclone was stronger, resulting in an enhancement of the subtropical jet south of the CONUS and below-average tornado totals ($\alpha = 0.05$; Figs. 12c,d). Southward subtropical jet stream positioning could also contribute to negative GoM basin SSTAs due to increased cloud cover over the GoM (Park and Leovy 2004). Future studies will explore whether very strong El Niño events tend to result in the subtropical jet stream being positioned south of the CONUS, or if the subtropical jet stream mean perturbation during the 1997–98 El Niño event was an anomaly.

### e. Alternative Niño regions

In an effort to better understand tornado variability that deviates from the relationships identified thus far with ENSO classified using ONI, other regions beyond Niño-3.4 were explored for potential influences on DJF tornado variability. Results show that the Niño-3 index relationship with DJF significant tornado variability (Fig. 13) is comparable to the relationship identified with ONI (Fig. 6). Strongly positive and negative Niño-3 region SSTAs, characteristic of El Niño and La Niña conditions, respectively, can result in significant tornado occurrences above the DJF mean (Fig. 13a). Higher significant tornado frequency in December is generally influenced by strongly positive and negative Niño-3 region SSTAs, while January and February are influenced by negative Niño-3 region SSTAs (Figs. 13b–d). The Niño-4 region, Niño-1+2 region, and Modoki index (Ashok et al. 2007) were also explored for potential teleconnections to DJF seasonal and subseasonal tornado variability, but the results were inconclusive (not shown). The similarities between the Niño-3 index and ONI relationships with DJF tornado variability suggest that both indices capture ENSO-driven modulations on CONUS tornado activity rather analogously, at both seasonal and monthly time scales.

## 4. Conclusions

Results herein show that El Niño, La Niña, and positive GoM SSTAs are related to increased DJF tornado frequencies and significant tornado environments across areas east of the Rocky Mountains. Greater tornado frequencies and intensities occur during both El Niño
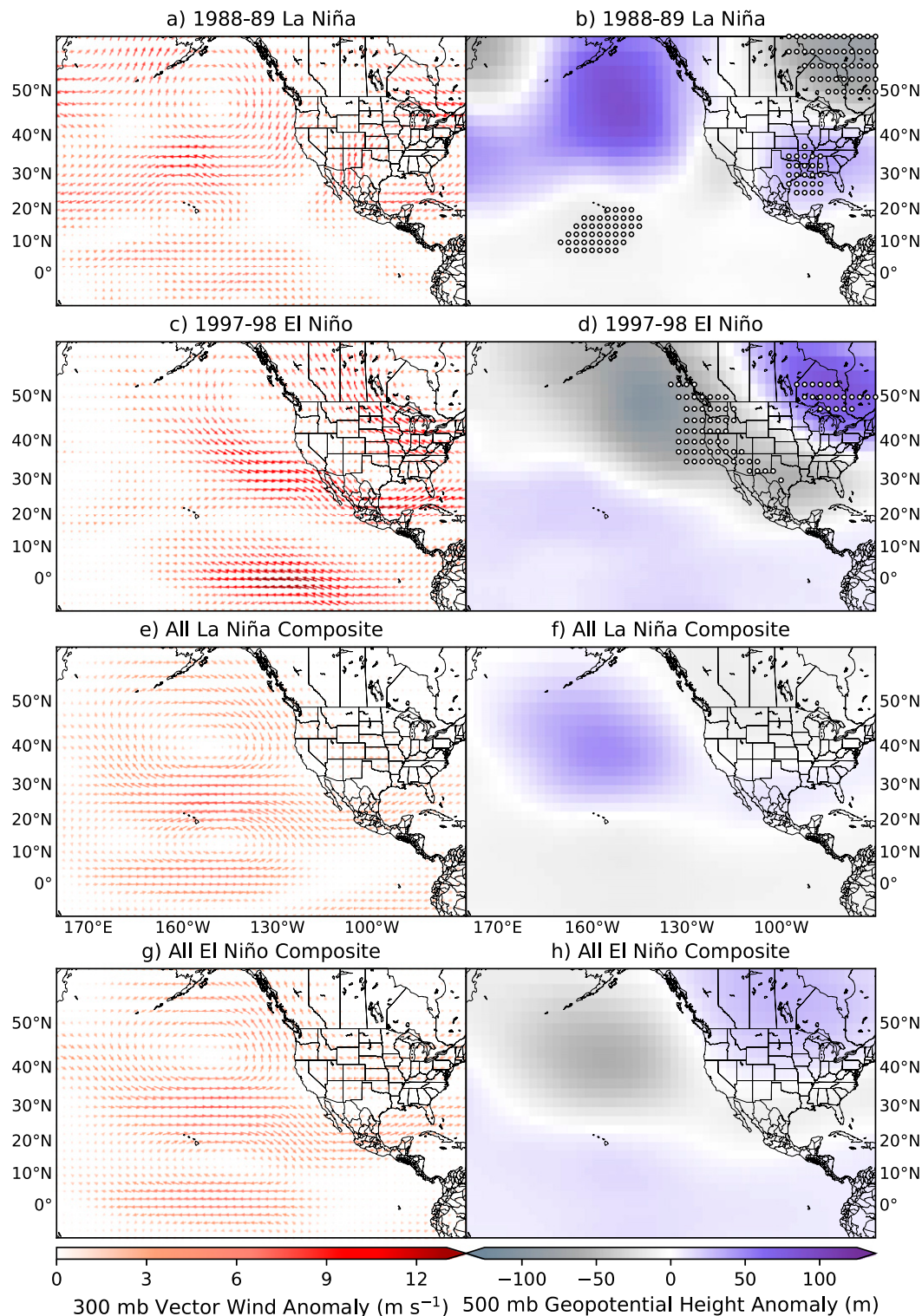
FIG. 12. Mean DJF (left) 300-hPa vector wind and (right) 500-hPa geopotential height anomalies for the (a),(b) 1988–89 La Niña and (c),(d) 1997–98 El Niño computed from the corresponding ENSO phase climatology (1979–2016), with statistical significance ($\alpha = 0.05$), as in Fig. 1, and for the (e),(f) La Niña and (g),(h) El Niño climatologies, which consist of 13 La Niña events and 13 El Niño events, respectively.
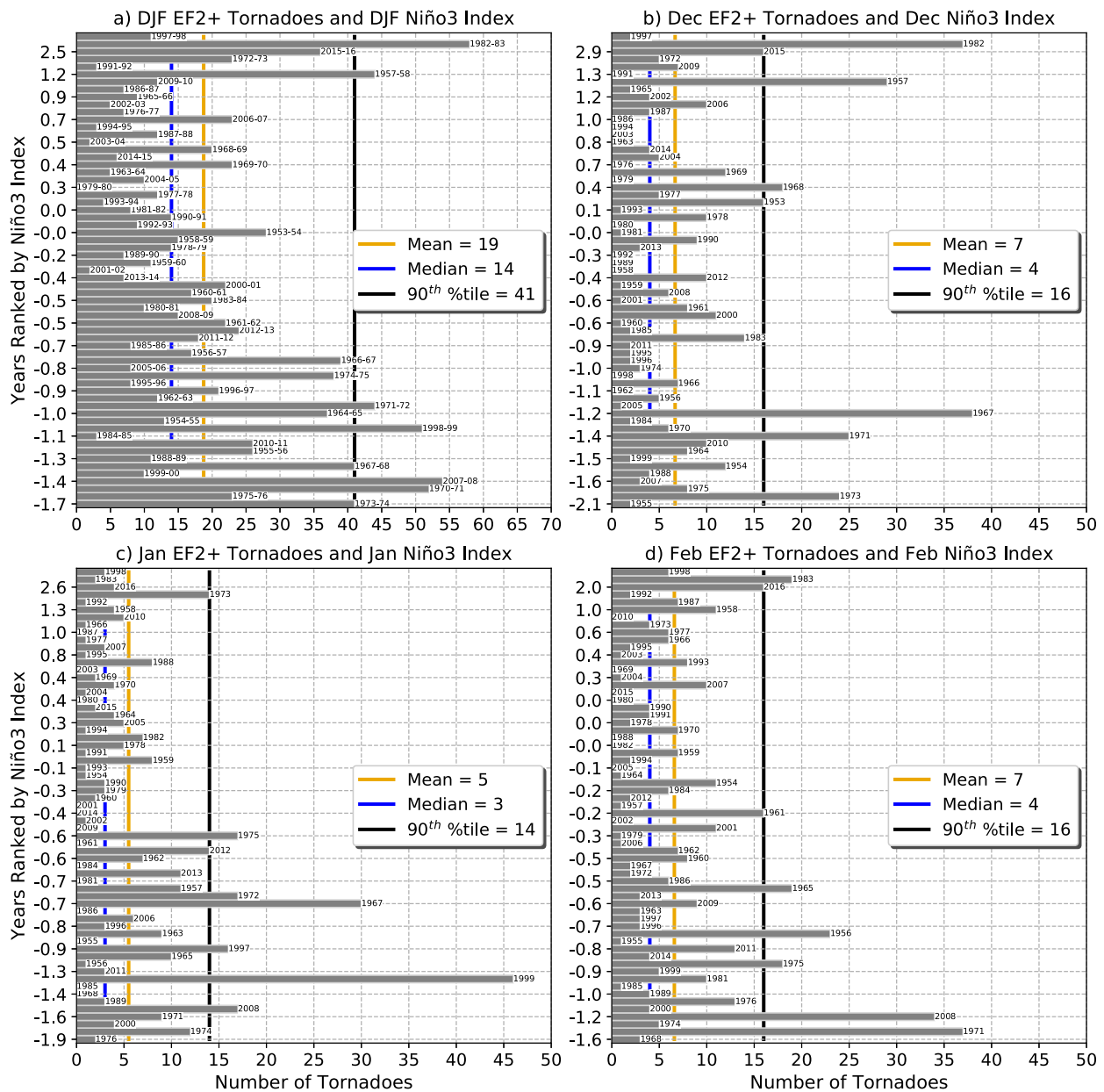
FIG. 13. DJF and monthly significant (EF2+) tornadoes for the contiguous United States ranked by (a) mean DJF (for DJF), (b) December, (c) January, and (d) February Niño-3 index values (1953–2016). The legend is as in Fig. 6.

and La Niña, but more so during La Niña than El Niño. Sensitivity to ENSO intensity was also identified; stronger El Niño and La Niña events occurred in conjunction with greater increases in favorable significant tornado environments, with El Niño related to increases in the SE-US, and La Niña related to increases in the Midwest and Midsouth. However, the La Niña (El Niño) influence on tornado frequency is sensitive to the positioning and intensity of the northeastern Pacific anticyclone (cyclone), with unfavorable polar jet (subtropical jet) perturbations potentially resulting in below-

average tornado totals across the CONUS. The large variance of DJF tornado totals during strong El Niño and La Niña events is illustrative of the internal variability of ENSO and associated downstream climate impacts. Significant tornado environments were also found to be influenced by anomalously warm and cool GoM SSTs, particularly in areas proximal to the GoM. It is important to note that warmer (cooler) surface waters in the GoM LC region increase (decrease) the daily probability of STP $\geq$ 1 across the SE-US. On the subseasonal scale, larger significant tornado totals are associated

with El Niño during December and La Niña during January and February, especially when concurrent with warm GoM SSTs.

To date, seasonal and subseasonal severe thunderstorm prediction efforts have focused on the MAM season (e.g., Allen et al. 2015; Lepore et al. 2017). However, DJF tornadoes impose a markedly perilous threat, as elucidated by Sherburn et al. (2016). Tornadoes are more frequently rated significant in DJF than in other seasons, a notable statistic given that significant tornadoes account for the vast majority of tornado fatalities, whether considering all seasons (95%) or isolating DJF (94%). Childs et al. (2018) found DJF tornado occurrences and favorable tornado environments to be on the rise across the SE-US, a region Ashley and Strader (2016) found to have a growing population exposed to tornado events. Thus, seasonal and subseasonal tornado forecasting efforts should expand to consider the DJF season using ENSO and the GoM as predictors.

A set of coupled dynamical models, together known as the North American Multimodel Ensemble (NMME; Kirtman et al. 2014), are often used for predictions of SSTs in the Niño-3.4 region. The NMME has been shown to skillfully predict DJF ONI with a lead time of 5 months (Barnston et al. 2017) and was recently shown to also have skill in forecasts using various ENSO intensity categories, such as moderate and strong (Tippett et al. 2017). The NMME also yields skillful GoM SST predictions (Becker et al. 2014; Hervieux et al. 2017), with reliable 4-week-lead-time forecasts for LC position and LC–WCR separation events already conducted using a neural network-based model (Zeng et al. 2015). Using an approach similar to that of Allen et al. (2015) and Lepore et al. (2017), categorical forecasts for DJF tornado occurrence can be developed using NMME forecast ONI and GoM SST values to predict whether the upcoming season will be above, below, or near average. Subseasonal forecasts can be developed analogously to provide more information about the predicted seasonal evolution of tornado activity. Future work will develop these seasonal and subseasonal forecasts and determine their skill using hindcasts.

It is important to acknowledge that, while ENSO and the GoM can help to identify deviations from the mean DJF seasonal and subseasonal climatology, severe thunderstorms and tornadoes are driven by meteorological processes and baroclinic systems with unique characteristics. A mean DJF environment favorable (unfavorable) for significant tornadoes is no guarantee that significant tornadoes will be above (below) average for that season or subseason. The greater variance in DJF tornado frequency associated with strong El Niño and La Niña events is also indicative that there is a higher potential for erroneous DJF seasonal

tornado forecasts during strong ENSO phases. However, DJF predictions that extend beyond the current SPC categorical convective storm outlooks could serve as an opportunity to communicate the dangers associated with DJF severe convective events to the public, with the aim of increasing preparedness and reducing fatalities in association with severe thunderstorms. The ultimate aim of better understanding seasonal and subseasonal severe thunderstorm activity and associated hazards will contribute to NOAA's National Weather Service vision for a Weather-Ready Nation (Lindell and Brooks 2013).

## REFERENCES

Alexander, M. A., I. Bladé, M. Newman, J. R. Lanzante, N.-C. Lau, and J. D. Scott, 2002: The atmospheric bridge: The influence of ENSO teleconnections on air–sea interaction over the global oceans. *J. Climate*, **15**, 2205–2231, https://doi.org/10.1175/1520-0442(2002)015<2205:TABTIO>2.0.CO;2.

Allard, J., J. V. Clarke III, and B. D. Keim, 2016: Spatial and temporal patterns of in situ sea surface temperatures within the Gulf of Mexico from 1901-2010. *Amer. J. Climate Change*, **5**, 69733, https://doi.org/10.4236/ajcc.2016.53025.

Allen, J. T., M. K. Tippett, and A. H. Sobel, 2015: Influence of the El Niño–Southern Oscillation on tornado and hail frequency in the United States. *Nat. Geosci.*, **8**, 278–283, https://doi.org/10.1038/ngeo2385.

——, M. J. Molina, and V. A. Gensini, 2018: Modulation of annual cycle of tornadoes by El Niño–Southern Oscillation. *Geophys. Res. Lett.*, **45**, 5708–5717, https://doi.org/10.1029/2018GL077482.

Ashley, W. S., 2007: Spatial and temporal analysis of tornado fatalities in the United States: 1880–2005. *Wea. Forecasting*, **22**, 1214–1228, https://doi.org/10.1175/2007WAF2007004.1.

——, and S. M. Strader, 2016: Recipe for disaster: How the dynamic ingredients of risk and exposure are changing the tornado disaster landscape. *Bull. Amer. Meteor. Soc.*, **97**, 767–786, https://doi.org/10.1175/BAMS-D-15-00150.1.

Ashok, K., S. K. Behera, S. A. Rao, H. Weng, and T. Yamagata, 2007: El Niño Modoki and its possible teleconnection. *J. Geophys. Res.*, **112**, C11007, https://doi.org/10.1029/2006JC003798.

Barlow, M., S. Nigam, and E. Berbery, 2001: ENSO, Pacific decadal variability, and U.S. summertime precipitation, drought, and stream flow. *J. Climate*, **14**, 2105–2128, https://doi.org/10.1175/1520-0442(2001)014<2105:EPDVAU>2.0.CO;2.

Barnston, A. G., M. Chelliah, and S. B. Goldenberg, 1997: Documentation of a highly ENSO-related SST region in the equatorial Pacific. *Atmos.–Ocean*, **35**, 367–383, https://doi.org/10.1080/07055900.1997.9649597.

——, M. K. Tippett, M. Ranganathan, and M. L. L'Heureux, 2017: Deterministic skill of ENSO predictions from the North American Multimodel Ensemble. *Climate Dyn.*, https://doi.org/10.1007/s00382-017-3603-3, in press.

Becker, E., H. van den Dool, and Q. Zhang, 2014: Predictability and forecast skill in NMME. *J. Climate*, **27**, 5891–5906, https://doi.org/10.1175/JCLI-D-13-00597.1.

Bjerknes, J., 1969: Atmospheric teleconnections from the equatorial Pacific. *Mon. Wea. Rev.*, **97**, 163–172, https://doi.org/10.1175/1520-0493(1969)097<0163:ATFTEP>2.3.CO;2.

Brooks, H., and C. A. Doswell III, 2001: Some aspects of the international climatology of tornadoes by damage classification. *Atmos. Res.*, **56**, 191–201, https://doi.org/10.1016/S0169-8095(00)00098-3.

——, ——, and J. Cooper, 1994: On the environments of tornadic and nontornadic mesocyclones. *Wea. Forecasting*, **9**, 606–618, https://doi.org/10.1175/1520-0434(1994)009<0606:OTEOTA>2.0.CO;2.

——, ——, and M. P. Kay, 2003: Climatological estimates of local daily tornado probability for the United States. *Wea. Forecasting*, **18**, 626–640, https://doi.org/10.1175/1520-0434(2003)018<0626:CEOLDT>2.0.CO;2.

——, G. W. Carbin, and P. T. Marsh, 2014: Increased variability of tornado occurrence in the United States. *Science*, **346**, 349–352, https://doi.org/10.1126/science.1257460.

Chang, Y.-L., and L. Oey, 2010: Eddy and wind-forced heat transports in the Gulf of Mexico. *J. Phys. Oceanogr.*, **40**, 2728–2742, https://doi.org/10.1175/2010JPO4474.1.

Childs, S. J., R. S. Schumacher, and J. T. Allen, 2018: Cold-season tornadoes: Climatological and meteorological insights. *Wea. Forecasting*, **33**, 671–691, https://doi.org/10.1175/WAF-D-17-0120.1.

Cohen, A. E., S. M. Cavallo, M. C. Coniglio, and H. E. Brooks, 2015: A review of planetary boundary layer parameterization schemes and their sensitivity in simulating southeastern U.S. cold season severe weather environments. *Wea. Forecasting*, **30**, 591–612, https://doi.org/10.1175/WAF-D-14-00105.1.

——, ——, ——, ——, and I. L. Jirak, 2017: Evaluation of multiple planetary boundary layer parameterization schemes in southeast U.S. cold season severe thunderstorm environments. *Wea. Forecasting*, **32**, 1857–1884, https://doi.org/10.1175/WAF-D-16-0193.1.

Cook, A. R., and J. T. Schaefer, 2008: The relation of El Niño–Southern Oscillation (ENSO) to winter tornado outbreaks. *Mon. Wea. Rev.*, **136**, 3121–3137, https://doi.org/10.1175/2007MWR2171.1.

——, L. M. Leslie, D. B. Parsons, and J. T. Schaefer, 2017: The impact of the El Niño–Southern Oscillation (ENSO) on winter and early spring U.S. tornado outbreaks. *J. Appl. Meteor. Climatol.*, **56**, 2455–2478, https://doi.org/10.1175/JAMC-D-16-0249.1.

CPC, 2015: Monthly atmospheric and SST indices. Climate Prediction Center, accessed December 2017, http://www.cpc.ncep.noaa.gov/data/indices/.

Doswell, C. A., III, 2007: Small sample size and data quality issues illustrated using tornado occurrence data. *Electron. J. Severe Storms Meteor.*, **2** (5), http://www.ejssm.org/ojs/index.php/ejssm/article/viewarticle/26/27.

——, and D. W. Burgess, 1988: On some issues of United States tornado climatology. *Mon. Wea. Rev.*, **116**, 495–501, https://doi.org/10.1175/1520-0493(1988)116<0495:OSIOUS>2.0.CO;2.

——, H. E. Brooks, and N. Dotzek, 2009: On the implementation of the enhanced Fujita scale in the USA. *Atmos. Res.*, **93**, 554–563, https://doi.org/10.1016/j.atmosres.2008.11.003.

Edwards, R., and S. J. Weiss, 1996: Comparisons between Gulf of Mexico sea surface temperature anomalies and southern US severe thunderstorm frequency in the cool season. Preprints, *18th Conf. on Severe Local Storms*, San Francisco, CA, Amer. Meteor. Soc., 19–23.

——, J. G. LaDue, J. T. Ferree, K. Scharfenberg, C. Maier, and W. L. Coulbourne, 2013: Tornado intensity estimation: Past, present, and future. *Bull. Amer. Meteor. Soc.*, **94**, 641–653, https://doi.org/10.1175/BAMS-D-11-00006.1.

Elsner, J. B., and H. M. Widen, 2014: Predicting spring tornado activity in the central Great Plains by 1 March. *Mon. Wea. Rev.*, **142**, 259–267, https://doi.org/10.1175/MWR-D-13-00014.1.

Fujita, T. T., 1971: Proposed characterization of tornadoes and hurricanes by area and intensity. University of Chicago SMRP Research Paper 91, 42 pp., https://archive.org/details/nasa_techdoc_19720008829.

Fye, F. K., D. W. Stahle, and E. R. Cook, 2004: Twentieth-century sea surface temperature patterns in the Pacific during decadal moisture regimes over the United States. *Earth Interact.*, **8**, https://doi.org/10.1175/1087-3562(2004)8<1:TSSTPI>2.0.CO;2.

Galway, J. G., and A. Pearson, 1981: Winter tornado outbreaks. *Mon. Wea. Rev.*, **109**, 1072–1080, https://doi.org/10.1175/1520-0493(1981)109<1072:WTO>2.0.CO;2.

Gensini, V. A., and A. Marinaro, 2016: Tornado frequency in the United States related to global relative angular momentum. *Mon. Wea. Rev.*, **144**, 801–810, https://doi.org/10.1175/MWR-D-15-0289.1.

——, T. L. Mote, and H. E. Brooks, 2014: Severe-thunderstorm reanalysis environments and collocated radiosonde observations. *J. Appl. Meteor. Climatol.*, **53**, 742–751, https://doi.org/10.1175/JAMC-D-13-0263.1.

Grams, J. S., R. L. Thompson, D. V. Snively, J. A. Prentice, G. M. Hodges, and L. J. Reames, 2012: A climatology and comparison of parameters for significant tornado events in the United States. *Wea. Forecasting*, **27**, 106–123, https://doi.org/10.1175/WAF-D-11-00008.1.

Guyer, J. L., D. A. Imy, and A. Kis, 2006: Cool season significant (F2-F5) tornadoes in the Gulf Coast states. *23rd Conf. on Severe Local Storms*, St. Louis, MO, Amer. Meteor. Soc., 4.2, https://ams.confex.com/ams/23SLS/techprogram/paper_115320.htm.

Hervieux, G., M. Alexander, C. Stock, M. Jacox, K. Pegion, E. Becker, F. Castruccio, and D. Tommasi, 2017: More reliable coastal SST forecasts from the North American multimodel ensemble. *Climate Dyn.*, https://doi.org/10.1007/s00382-017-3652-7, in press.

Huang, B., and Coauthors, 2017: Extended Reconstructed Sea Surface Temperature, version 5 (ERSSTv5): Upgrades, validations, and intercomparisons. *J. Climate*, **30**, 8179–8205, https://doi.org/10.1175/JCLI-D-16-0836.1.

Kanamitsu, M., W. Ebisuzaki, J. Woollen, S.-K. Yang, J. Hnilo, M. Fiorino, and G. Potter, 2002: NCEP–DOE AMIP-II Reanalysis (R-2). *Bull. Amer. Meteor. Soc.*, **83**, 1631–1643, https://doi.org/10.1175/BAMS-83-11-1631.

King, J. R., M. D. Parker, K. D. Sherburn, and G. M. Lackmann, 2017: Rapid evolution of cool season, low-CAPE severe thunderstorm environments. *Wea. Forecasting*, **32**, 763–779, https://doi.org/10.1175/WAF-D-16-0141.1.

Kirtman, B. P., and Coauthors, 2014: The North American Multimodel Ensemble: Phase-1 seasonal-to-interannual prediction; phase-2 toward developing intraseasonal prediction. *Bull. Amer. Meteor. Soc.*, **95**, 585–601, https://doi.org/10.1175/BAMS-D-12-00050.1.

Kis, A. K., and J. M. Straka, 2010: Nocturnal tornado climatology. *Wea. Forecasting*, **25**, 545–561, https://doi.org/10.1175/2009WAF2222294.1.

Klazura, G. E., and D. A. Imy, 1993: A description of the initial set of analysis products available from the NEXRAD WSR-88D system. *Bull. Amer. Meteor. Soc.*, **74**, 1293–1311, https://doi.org/10.1175/1520-0477(1993)074<1293:ADOTIS>2.0.CO;2.

Knowles, J. B., and R. A. Pielke Sr., 2005: Southern Oscillation and its effect on tornadic activity in the United States. Colorado State University Dept. of Atmospheric Science Paper 755, 11 pp., https://pielkeclimatesci.files.wordpress.com/2009/09/nr-141.pdf.

Krocak, M. J., and H. E. Brooks, 2018: Climatological estimates of hourly tornado probability for the United States. *Wea. Forecasting*, **33**, 59–69, https://doi.org/10.1175/WAF-D-17-0123.1.

Lee, J. T., and J. Galway, 1956: Preliminary report on the relationship between the jet at the 200-mb level and tornado occurrence. *Bull. Amer. Meteor. Soc.*, **37**, 327–332, https://doi.org/10.1175/1520-0477-37.7.327.

Lee, S.-K., A. T. Wittenberg, D. B. Enfield, S. J. Weaver, C. Wang, and R. Atlas, 2016: US regional tornado outbreaks and their links to spring ENSO phases and North Atlantic SST variability. *Environ. Res. Lett.*, **11**, 044008, https://doi.org/10.1088/1748-9326/11/4/044008.

Lepore, C., M. K. Tippett, and J. T. Allen, 2017: ENSO-based probabilistic forecasts of March–May US tornado and hail activity. *Geophys. Res. Lett.*, **44**, 9093–9101, https://doi.org/10.1002/2017GL074781.

L'Heureux, M. L., M. K. Tippett, and A. G. Barnston, 2015: Characterizing ENSO coupled variability and its impact on North American seasonal precipitation and temperature. *J. Climate*, **28**, 4231–4245, https://doi.org/10.1175/JCLI-D-14-00508.1.

Lindell, M. K., and H. Brooks, 2013: Workshop on weather ready nation: Science imperatives for severe thunderstorm research. *Bull. Amer. Meteor. Soc.*, **94**, ES171–ES174, https://doi.org/10.1175/BAMS-D-12-00238.1.

Mercer, A. E., C. M. Shafer, C. A. Doswell III, L. M. Leslie, and M. B. Richman, 2012: Synoptic composites of tornadic and nontornadic outbreaks. *Mon. Wea. Rev.*, **140**, 2590–2608, https://doi.org/10.1175/MWR-D-12-00029.1.

Mesinger, F., and Coauthors, 2006: North American Regional Reanalysis. *Bull. Amer. Meteor. Soc.*, **87**, 343–360, https://doi.org/10.1175/BAMS-87-3-343.

Molina, M., R. Timmer, and J. Allen, 2016: Importance of the Gulf of Mexico as a climate driver for US severe thunderstorm activity. *Geophys. Res. Lett.*, **43**, 12 295–12 304, https://doi.org/10.1002/2016GL071603.

Montroy, D. L., 1997: Linear relation of central and eastern North American precipitation to tropical Pacific sea surface temperature anomalies. *J. Climate*, **10**, 541–558, https://doi.org/10.1175/1520-0442(1997)010<0541:LROCAE>2.0.CO;2.

Muller-Karger, F. E., and Coauthors, 2015: Natural variability of surface oceanographic conditions in the offshore Gulf of Mexico. *Prog. Oceanogr.*, **134**, 54–76, https://doi.org/10.1016/j.pocean.2014.12.007.

Park, S., and C. B. Leovy, 2004: Marine low-cloud anomalies associated with ENSO. *J. Climate*, **17**, 3448–3469, https://doi.org/10.1175/1520-0442(2004)017<3448:MLAAWE>2.0.CO;2.

Pautz, M. E., 1969: Severe local storm occurrences 1955–1967. ESSA Tech. Memo. WBTM FCST12, 77 pp.

Potter, S., 2007: Fine-tuning Fujita: After 35 years, a new scale for rating tornadoes takes effect. *Weatherwise*, **60** (2), 64–71, https://doi.org/10.3200/WEWI.60.2.64-71.

Rasmussen, E. N., and D. O. Blanchard, 1998: A baseline climatology of sounding-derived supercell and tornado forecast parameters. *Wea. Forecasting*, **13**, 1148–1164, https://doi.org/10.1175/1520-0434(1998)013<1148:ABCOSD>2.0.CO;2.

Reynolds, R. W., T. M. Smith, C. Liu, D. B. Chelton, K. S. Casey, and M. G. Schlax, 2007: Daily high-resolution-blended analyses for sea surface temperature. *J. Climate*, **20**, 5473–5496, https://doi.org/10.1175/2007JCLI1824.1.

Ropelewski, C. F., and M. S. Halpert, 1986: North American precipitation and temperature patterns associated with the El Niño–Southern Oscillation (ENSO). *Mon. Wea. Rev.*, **114**, 2352–2362, https://doi.org/10.1175/1520-0493(1986)114<2352:NAPATP>2.0.CO;2.

Schaefer, J. T., and R. Edwards, 1999: The SPC tornado/severe thunderstorm database. Preprints, *11th Conf. on Applied Climatology*, Dallas, TX, Amer. Meteor. Soc., 215–220.

——, R. S. Schneider, and M. P. Kay, 2002: The robustness of tornado hazard estimates. *Third Symp. on Environmental Applications*, Orlando, FL, Amer. Meteor. Soc., 4.2, https://ams.confex.com/ams/annual2002/techprogram/paper_27694.htm.

Sherburn, K. D., and M. D. Parker, 2014: Climatology and ingredients of significant severe convection in high-shear, low-CAPE environments. *Wea. Forecasting*, **29**, 854–877, https://doi.org/10.1175/WAF-D-13-00041.1.

——, ——, J. R. King, and G. M. Lackmann, 2016: Composite environments of severe and nonsevere high-shear, low-CAPE convective events. *Wea. Forecasting*, **31**, 1899–1927, https://doi.org/10.1175/WAF-D-16-0086.1.

Smith, B. T., R. L. Thompson, J. S. Grams, C. Broyles, and H. E. Brooks, 2012: Convective modes for significant severe thunderstorms in the contiguous United States. Part I: Storm classification and climatology. *Wea. Forecasting*, **27**, 1114–1135, https://doi.org/10.1175/WAF-D-11-00115.1.

Thompson, R. L., R. Edwards, J. A. Hart, K. L. Elmore, and P. Markowski, 2003: Close proximity soundings within supercell environments obtained from the Rapid Update Cycle. *Wea. Forecasting*, **18**, 1243–1261, https://doi.org/10.1175/1520-0434(2003)018<1243:CPSWSE>2.0.CO;2.

Tippett, M. K., J. T. Allen, V. A. Gensini, and H. E. Brooks, 2015: Climate and hazardous convective weather. *Curr. Climate Change Rep.*, **1**, 60–73, https://doi.org/10.1007/s40641-015-0006-6.

——, M. Ranganathan, M. L'Heureux, A. G. Barnston, and T. DelSole, 2017: Assessing probabilistic predictions of ENSO phase and intensity from the North American Multimodel Ensemble. *Climate Dyn.*, https://doi.org/10.1007/s00382-017-3721-y, in press.

Trenberth, K. E., 1997: The definition of El Niño. *Bull. Amer. Meteor. Soc.*, **78**, 2771–2777, https://doi.org/10.1175/1520-0477(1997)078<2771:TDOENO>2.0.CO;2.

Verbout, S. M., H. E. Brooks, L. M. Leslie, and D. M. Schultz, 2006: Evolution of the U.S. tornado database: 1954–2003. *Wea. Forecasting*, **21**, 86–93, https://doi.org/10.1175/WAF910.1.

Vukovich, F. M., 2007: Climatology of ocean features in the Gulf of Mexico using satellite remote sensing data. *J. Phys. Oceanogr.*, **37**, 689–707, https://doi.org/10.1175/JPO2989.1.

Weiss, S. J., 1992: Some aspects of forecasting severe thunderstorms during cool-season return-flow episodes. *J. Appl. Meteor.*, **31**, 964–982, https://doi.org/10.1175/1520-0450(1992)031<0964:SAOFST>2.0.CO;2.

Zavala-Hidalgo, J., A. Parés-Sierra, and J. Ochoa, 2002: Seasonal variability of the temperature and heat fluxes in the Gulf of Mexico. *Atmósfera*, **15**, 81–104.

Zeng, X., Y. Li, and R. He, 2015: Predictability of the Loop Current variation and eddy shedding process in the Gulf of Mexico using an artificial neural network approach. *J. Atmos. Oceanic Technol.*, **32**, 1098–1111, https://doi.org/10.1175/JTECH-D-14-00176.1.